EVALUATION OF A SIMPLE COMPUTATIONAL FLUID DYNAMICS (CFD) URBAN WIND MODEL IN A COMPLEX VEGETATED URBAN AREA

by

Hanieh Eshagh

A thesis submitted to the faculty of
The University of Utah
in partial fulfillment of the requirements for the degree of

Master of Science

Department of Mechanical Engineering

The University of Utah

December 2017

Copyright © Hanieh Eshagh 2017
All Rights Reserved

The University of Utah Graduate School

STATEMENT OF THESIS APPROVAL

The thesis of **Hanieh Eshagh**

has been approved by the following supervisory committee members:

Eric R. Pardyjak	, Chair	**5/31/2017** Date Approved
James R. Stoll	, Member	Date Approved
Marc Calaf	, Member	**9/6/2017** Date Approved

and by **Tim Ameel** , Chair/Dean of

the Department/College/School of **Mechanical Engineering**

and by David B. Kieda, Dean of The Graduate School.

ABSTRACT

While it is well accepted that modeling of vegetation in urban areas is important for simulating urban microclimate, most well-known urban models have neglected vegetation, particularly explicit modeling of vegetation elements such as trees. In this study, we quantitatively evaluate mean wind fields generated using the building-resolving Quick Urban Industrial Complex wind model (QUIC-URB) for an urban domain containing a high vegetation fraction, including a large number of trees. A new vegetation model that has both theoretical and empirical features is developed. The performance of this new vegetation model is compared with published wind-tunnel data available in literature and the results show less than 15% relative deviations. Further evaluation is done using mean wind data from a suite of eleven low-cost weather stations that were distributed throughout the University of Utah campus during a 2-year period, from 2015 to 2017. Results are presented for simulations with and without vegetation using different configurations of QUIC's standard canopy vegetation model as well as the newly developed isolated tree model. Preliminary modeling results indicate underestimation of wind speeds in the upwind cavity and building wake zones. However, the outcomes of the newly developed model are in a good agreement with the observed experimental trends in wide open areas and street-canyon regions.

For teaching me how to work, for pushing me to be my best,
and for never ceasing to amaze and encourage me,
I dedicate this to my wonderful parents.

CONTENTS

LIST OF FIGURES

LIST OF TABLES

ACKNOWLEDGMENTS

First and foremost, I would like to express my sincere gratitude to my advisor Prof. Eric Pardyjak for the patient guidance, encouragement, and immense advice he has provided throughout this research. I have been extremely lucky to have a supervisor who cared so much about my research.

My special thanks and appreciation goes to Dr. Rob Stoll for his guidance, collaboration, and insightful advice.

I gratefully acknowledge the funding sources that made my research work possible. I was funded by the National Science Foundation and the University of Utah Graduate assistantship.

Thanks to my colleagues and fellow researchers Arash Nemati Hayati, Nipun Gunawardena, Nate Miller, Tim Price, Anup Khadka, and Mohammad Khan for their help during the research work.

Very special thanks to my fiance (Alireza Asiaee) for his immense love and encouragement.

Last but not least, words alone cannot describe the deep gratitude I owe to my parents (Shahrzad Panahi and Majid Eshagh) and my siblings (Foziah and Farhad) for their unconditional love, support, encouragement, and by always believing in me.

This material is based in part upon work supported by the National Science Foundation under Grant Number CBET 1512740: *Localized Distributed Power Generation: Economically Robust, Demand-Optimized Placement of Urban Energy Production Systems* project.

CHAPTER 1

INTRODUCTION

Vegetation and trees are critical parts of urban ecology (Pataki et al., 2006). They not only have design-based benefits for cities but also play a critical role in modulating the air quality of metropolitan areas (Nowak and Heisler, 2010). Carbon sequestration (Nowak and Crane, 2002), mitigation of the urban heat island (UHI) effect (Akbari et al., 2001; Salim et al., 2015), and filtering of aerosol pollutants by deposition processes (Akbari, 2009) are among the most well-known ecosystem services provided by trees. Nowak et al. (2006) estimated that urban trees can remove 711,000 metric tons annually of total air pollutant particles, which is equivalent to $3.8 billion in economic benefits. Moreover, urban vegetation can intercept rainfall to help control stormwater runoff (Xiao et al., 1998), provide wind barriers to control erosion (Gyssels et al., 2005), reduce wind speeds for shielding buildings, and provide shading and evapotranspiration (Kurn et al., 1994) for modulating thermal comfort (Akbari, 2009). As a result of these effects, vegetation can modulate energy consumption of residential and commercial buildings. Hence, urban trees have the potential to directly reduce energy loss and help mitigate various types of pollution. These benefits vary based on the density of canopy cover, size, population, and other topographical features of specific areas. Table 1.1 shows an estimate of urban tree density for selected U.S. cities. This estimate is based on the National Land Cover Database (NLCD), which uses satellite imagery to approximate the current surface cover (Nowak et al., 2010). Because of an error in their method, the actual urban tree density is expected to be even higher. The average tree density in some U.S. cities varies from about 23 trees per hectare in Casper, Wyoming, to 275 trees per hectare in Atlanta, GA (Nowak et al., 2008). The potential climate and economic benefits of these vegetative

landscaping elements is of interest to ecologists, physicists, engineers, urban planners, and even utility companies (McPherson, 1996). Additionally, worldwide urbanization patterns (Grimm et al., 2008) continue to put pressure on energy resources, leading to a need to develop a systematic knowledge of land cover and ecosystem behaviours in these areas. As a result, there have been many studies in recent years focused on understanding the impact of landscaping and green infrastructure in general in urban areas.

Most urban wind modeling studies only consider the morphological impacts of buildings and neglect other elements (Grimmond et al., 2011), in spite of the fact that other stationary elements such as trees or even nonstationary objects such as moving vehicles might have a notable effect on the urban environment (Mochida and Lun, 2008). Most studies account for the impact of trees through a modified surface roughness. However, to better understand their various impacts, canopies should be resolved explicitly (Salim et al., 2015). Explicitly resolving vegetative canopies requires detailed knowledge of their structural characteristics such as geometry and leaf area density (Salim et al., 2015). This is a big challenge because the measurement of these features can be difficult and includes uncertainty due to seasonal changes (Chen, 1996; Mochida and Lun, 2008). In addition, canopy-resolving models should integrate microscale effects including the impacts of small-scale turbulence and the interaction of vegetation with its surroundings and mesoscales. The better a model integrates all of these effects, the better it can determine the actual characteristics of the flow (Salim et al., 2015). However, it has been a challenging task to develop such an integrated model for two main reasons. First, this type of tool requires fast-response modeling approaches so that many simulations can be run for planning and assessment purposes (Brown, 2004). Second, it has to be able to resolve street tree and leaf scales, which requires intensive computational resources. Among the many vegetated urban atmospheric boundary layer (ABL) configurations possible, there are two main classifications (suggested by Horne (2012)) which are of primary interest in this paper: first, dense urban canopies, and second, very sparse canopies with nearly isolated trees such as those typically found along streets and in parks.

Dense canopies have been the focus of many recent transport process studies

because of the wide variety of applications in agriculture (Finnigan, 2000; Cescatti and Marcolla, 2004; Cava et al., 2006; Poggi and Katul, 2007). Dense canopies are characterized by trees with heights much greater than the spacing of the individual plants. Pietri et al. (2009) discussed the effect of canopy density on turbulence characteristics within and above canopies by conducting experiments on both dense and sparse canopies. The dense canopy studies show two important flow features: first is a transverse Kelvin-Helmholtz wave, which results from an instability related to the inflected mean streamwise velocity profile. Large coherent eddies and turbulence that are generated in the wake of the canopy were studied by Raupach et al. (1996) and Finnigan (2000) to quantify the advantages of using plane mixing layer over boundary layer within the vegetated canopy. The second major feature is the spectral short cut in turbulent energy, which is the result of aerodynamic drag force within and above the foliage. This mechanism contributes to the energy cascade that transfers energy from large-scale eddies to fine scales (Finnigan, 2000; Poggi et al., 2004).

In addition to dense tree canopies, recent work has focused on other sparse canopy geometries such as windbreaks and forest clearings (Judd et al., 1996; Irvine et al., 1997; Miller et al., 2015; Poëtte et al., 2017). In this type of canopy, the horizontal spacing between plants is greater than the plant height. These types of canopies are valuable for controlling erosion and sheltering. Many research studies have been conducted to understand windbreaks and their impacts on atmospheric surface-layer flow fields. Plate (1971) studied the impact of windbreak aerodynamic features on velocity distributions in sheltered regions. McNaughton (1988) reviewed the effects of the quiet and wake zones in the lee of a windbreak. Heisler and Dewalle (1988) discussed different flow structures around windbreak caused by porosity, windbreak geometry, angle, and stability of the incident flow. Speckart and Pardyjak (2014) developed models for mean and fluctuating velocities around a windbreak and implemented them into a simple empirically-based CFD code. Judd et al. (1996) described the flow characteristics around single and multiple windbreaks. Guan et al. (2003) used wind-tunnel experiments to develop a model for drag force in windbreaks. However, to the authors' knowledge, very few publications have addressed the dynamics of flow around an isolated canopy. The existing studies consist of data from field campaigns,

wind tunnel experiments, and numerical modeling. Several field-experiment studies have illustrated the importance of vegetation. Mayaud et al. (2016) explored the effect of having a single tree, a grass clump, and a shrub on turbulent wind flow and showed the reduction of wind speed up to 70% in the lee of vegetation. Leenders et al. (2007) studied the wind speed pattern and wind soil erosion around five types of vegetation. Their results showed a reduction in wind speed close to the soil surface for shrubs, while for trees the wind speed was increased around the trunk. Wind-tunnel studies have been conducted using hot-wire measurements for flow around individual trees (Ohahsi, 2004), as well as Laser Doppler Velocimetry (LDV) (Ruck and Schmitt, 1986; Ruck and Adams, 1991; Gromke and Ruck, 2008) and Particle Image Velocimetry (PIV) for flow around fir (Lee et al., 2014) and polymer-based trees (Manikhathan et al., 2016). Using LDV Ruck and Adams (1991) measured the flow characteristics around a single tree, forests, and extended flat and hilly forests. Using the same method, Gromke and Ruck (2008) found that tree-wake flow characteristics are not a strong function of crown porosity. Numerical studies of sparse canopies have used different methods including: Reynolds Averaged Navier-Stokes (RANS) and Large-Eddy Simulation (LES) solvers. Gross (1987) developed a three-dimensional nonhydrostatic model to characterize turbulent airflow in sparse canopies. To study the impact of vegetation using RANS models, k-ε closure schemes are typically modified by adding extra terms in the momentum equation (Mochida et al., 2006; Yamaguchi et al., 2009). Using LES, Horne (2012), Fang et al. (2015), Bailey and Stoll (2013), Patton et al. (1995), and Finnigan et al. (2009) used a modeled drag force to represent the impacts of an isolated tree. They performed simulations and used the results to develop a parametrisation for streamwise velocity. Wind speed reduction and sheltering effects on the wake behind single and multiple porous obstacles were studied by Taylor and Salmon (1993) and Lemberg (1973). Lemberg (1973) proposed a Gaussian distribution to predict the mean velocity deficit theoretically and compared the results of the model with wind-tunnel experiments. He investigated mean and turbulent flow features around six obstacles by using wind-tunnel and hot wire techniques. He found a rapid decay in three-dimensional wakes compared to two-dimensional wakes. Taylor and Salmon (1993) studied the

wind speed reduction and shelter effects in the wake behind two-dimensional fences and three-dimensional porous obstacles by assuming a Gaussian distribution for 3D obstacles. They found that the wake moment coefficient is considerably larger for a 2D fence compared to a 3D object, which leads to a notable overestimation of sheltering effects in the Wind Atlas Analysis and Application Program (WAsP).

The present study explores the effects of vegetation canopies on the alteration of urban microclimate in highly vegetated areas. We use the Quick Urban Industrial Complex - Urban (QUIC-URB) model, a fast-response simple computational fluid dynamics (CFD) model, which uses empirical parametrisations along with the mass conservation to produce averaged three-dimensional wind fields (Pardyjak and Brown, 2002, 2003; Singh, 2010; Brown et al., 2013; Speckart and Pardyjak, 2014). A new parametrisation is introduced to simulate the physics of flow around and within an individual urban element (e.g., a tree). The new model is validated against published wind-tunnel studies and evaluated in a realistic sparse suburban setting (measurements taken from the University of Utah campus). The new model is compared with a no-vegetation canopy model and a bulk vegetation model, which comes in standard QUIC-URB releases (Amatul, 2006).

Table 1.1. Estimation of urban trees for selected cities in the U.S. (Nowak et al., 2008)

City	Trees density (no per hectare)	Trees land cover (%)
Atlanta, GA	275	36.7
San Francisco, CA	56	11.9
Casper, WY	23	8.9

1.1 References

Akbari, H., 2009: Cooling our communities. A guidebook on tree planting and light-colored surface. *Lawrence Berkeley National Laboratory*.

Akbari, H., M. Pomerantz, and H. Taha, 2001: Cool surfaces and shade trees to reduce energy use and improve air quality in urban areas. *Solar Energy*, **70 (3)**, 295 – 310.

Amatul, U., 2006: Implementation and validation of particle transport model for vegetation in QUIC Urban dispersion modelling system. Master thesis, University of Utah.

Bailey, B. N., and R. Stoll, 2013: Turbulence in sparse, organized vegetative canopies: A large-eddy simulation study. *Boundary-Layer Meteorology*, **147 (3)**, 369–400.

Brown, M., 2004: Urban dispersion- challenges for fast response modeling. *Fifth AMS Symposium on the Urban Environment*.

Brown, M. J., A. A. Gowardhan, M. A. Nelson, M. D. Williams, and E. R. Pardyjak, 2013: QUIC transport and dispersion modelling of two releases from the joint urban 2003 field experiment. *International Journal of Environment and Pollution*, **52 (3-4)**, 263–287.

Cava, D., G. Katul, A. Scrimieri, D. Poggi, A. Cescatti, and U. Giostra, 2006: Buoyancy and the sensible heat flux budget within dense canopies. *Boundary-Layer Meteorology*, **118**, 217– 240.

Cescatti, A., and B. Marcolla, 2004: Drag coefficient and turbulence intensity in conifer canopies. *Agricultural and Forest Meteorology*, **121**, 197– 206.

Chen, J. M., 1996: Optically-based methods for measuring seasonal variation of leaf area index in boreal conifer stands. *Agricultural and Forest Meteorology*, **80 (2)**, 135 – 163.

Fang, F.-M., T.-C. Liang, C.-Y. Chung, and Y.-C. Li, 2015: On the simulation of flow around discrete coniferous trees. *Journal of the Chinese Institute of Engineers*, **38 (5)**, 665–674.

Finnigan, J., 2000: Turbulence in plant canopies. *Annual Review of Fluid Mechanics*, **32**, 519– 571.

Finnigan, J. J., R. H. Shaw, and E. G. Patton, 2009: Turbulence structure above a vegetation canopy. *Journal of Fluid Mechanics*, **637**, 387424.

Grimm, N. B., S. H. Faeth, N. E. Golubiewski, C. L. Redman, J. Wu, X. Bai, and J. M. Briggs, 2008: Global change and the ecology of cities. *Science*, **319 (5864)**, 756–760.

Grimmond, C. S. B., and Coauthors, 2011: Initial results from phase 2 of the international urban energy balance model comparison. *International Journal of Climatology*, **31 (2)**, 244–272.

Gromke, C., and B. Ruck, 2008: Aerodynamic modelling of trees for small-scale wind tunnel studies. *Forestry: An International Journal of Forest Research*, **81**, 243– 258.

Gross, G., 1987: A numerical study of the air flow within and around a single tree. *Boundary-Layer Meteorology*, **40**, 311– 327.

Guan, D., Y. Zhang, and T. Zhu, 2003: A wind-tunnel study of windbreak drag. *Agricultural and Forest Meteorology*, **118 (12)**, 75 – 84.

Gyssels, G., J. Poesen, E. Bochet, and Y. Li, 2005: Impact of plant roots on the resistance of soils to erosion by water: A review. *Progress in Physical Geography*, **29 (2)**, 189–217.

Heisler, G. M., and D. R. Dewalle, 1988: Effects of windbreak structure on wind flow. *Agriculture, Ecosystems & Environment*, **22**, 41 – 69.

Horne, W., 2012: Flow around a solitary tree in a large field under neutral atmospheric stratification. Master thesis, University of Utah.

Irvine, M. R., B. A. Gardiner, and M. K. Hill, 1997: The evolution of turbulence across a forest edge. *Boundary-Layer Meteorology*, **84 (3)**, 467–496.

Judd, M., M. Raupach, and J. Finnigan, 1996: A wind tunnel study of turbulent flow around single and multiple windbreaks, part 1: velocity fields. *Boundary-Layer Meteorology*, **80 (1)**, 127 – 165.

Kurn, D. M., S. E. Bretz, B. Huang, and H. Akbari, 1994: The potential for reducing urban air temperatures and energy consumption through vegetative cooling. *Lawrence Berkeley National Laboratory Report LBL-35320*.

Lee, J.-P., E.-J. Lee, and S.-J. Lee, 2014: Shelter effect of a fir tree with different porosities. *Journal of Mechanical Science and Technology*, **28 (2)**, 565–572.

Leenders, J., J. Van Boxel, and G. Sterk, 2007: The effect of single vegetation elements on wind speed and sediment transport in the sahelian zone of Burkina Faso. *Earth Surface Process and Landforms*, **32**, 1454– 1474.

Lemberg, R., 1973: On the wake behind bluff bodies in a turbulent boundary-layer. Phd thesis, Western University.

Manikhathan, L., T. Defraeye, J. Allegrini, D. Derome, and J. Carmeliet, 2016: Aerodynamic characterisation of model vegetation by wind tunnel experiments. *The fourth international conference on countermeasures to urban heat island*.

Mayaud, J. R., G. F. Wiggs, and R. M. Bailey, 2016: Characterizing turbulent wind flow around dryland vegetation. *Earth Surface Processes and Landforms*, **41 (10)**, 1421–1436.

McNaughton, K., 1988: Effects of windbreaks on turbulent transport and microclimate. *Agriculture, Ecosystems & Environment*, **22**, 17 – 39.

McPherson, E. R. R., 1996: Energy conservation potentioal of urban tree planting. *Journal of Arboriculture*, **19 (6)**, 321 – 331.

Miller, N. E., R. Stoll, W. F. Mahaffee, T. M. Neill, and E. R. Pardyjak, 2015: An experimental study of momentum and heavy particle transport in a trellised agricultural canopy. *Agricultural and Forest Meteorology*, **211-212**, 100 – 114.

Mochida, A., and I. Lun, 2008: Prediction of wind environment and thermal comfort at pedestrian level in urban area. *Journal of Wind Engineering and Industrial Aerodynamics*, **96 (10-11)**, 1498–1527.

Mochida, A., H. Yoshino, T. Iwata, and Y. Tabata, 2006: Optimization of tree canopy model for CFD prediction of wind environment at pedestrian level. *The Fourth International Symposium on Computational Wind Engineering*, **CWE2006**, 561–564.

Nowak, D., and D. Crane, 2002: Carbon storage and sequestration by urban trees in the USA. *Environmental Pollutant*, **116**, 381 – 389.

Nowak, D., and G. Heisler, 2010: Air quality effects of urban trees and parks. *National Recreation and Parks Association*.

Nowak, D. J., D. E. Crane, and J. C. Stevens, 2006: Air pollution removal by urban trees and shrubs in the United States. *Urban Forestry & Urban Greening*, **4 (34)**, 115 – 123.

Nowak, D. J., D. E. Crane, J. C. Stevens, R. E. Hoehn, J. T. Walton, and J. Bond, 2008: A ground-based method of assessing urban forest structure and ecosystem services. *Arboriculture and Urban Forestry*, **34 (6)**, 347 – 358.

Nowak, D. J., S. M. Stein, P. B. Randler, E. J. Greenfield, S. J. Comas, M. A. Carr, and R. J. Alig, 2010: Sustaining America's urban trees and forest: A forest on the edge report. *General Technical Report NRS-62*.

Ohahsi, M., 2004: A study on analysis of airflow around an individual tree. *Journal of Environmental Engineering*, **578**, 91– 96.

Pardyjak, E. R., and M. Brown, 2002: Fast response modeling of a two building urban street canyon. *4th AMS Symposium on the Urban Environment, Norfolk, VA, May*, 20– 24.

Pardyjak, E. R., and M. Brown, 2003: QUIC-URB v1.1 theory and user's guide. *Los Alamos National Laboratory, Los Alamos, NM*.

Pataki, D. E., and Coauthors, 2006: Urban ecosystems and the North American carbon cycle. *Global Change Biology*, **12 (11)**, 2092–2102.

Patton, E., R. Shaw, and K. T. Paw, 1995: Large-eddy simulation of a forest: Influence of canopy structure on turbulent kinetic energy. *11th Symposium on Boundary Layers and Turbulence*, **15 (2)**, 525–528.

Pietri, L., A. Petroff, M. Amielh, and F. Anselmet, 2009: Turbulence characteristics within sparse and dense canopies. *Environmental Fluid Mechanics*, **9 (3)**, 297.

Plate, E. J., 1971: The aerodynamics of shelter belts. *Agricultural Meteorology*, **8**, 203 – 222.

Poëtte, C., B. Gardiner, S. Dupont, I. Harman, M. Böhm, J. Finnigan, D. Hughes, and Y. Brunet, 2017: The impact of landscape fragmentation on atmospheric flow: A wind-tunnel study. *Boundary-Layer Meteorology*, **163 (3)**, 393–421.

Poggi, D., and G. Katul, 2007: An experimental investigation of the mean momentum budget inside dense canopies on narrow gentle hilly terrain. *Agricultural and Forest Meteorology*, **144**, 1– 13.

Poggi, D., A. Porporato, and L. Ridolfi, 2004: The effect of vegetation density on canopy sub-layer turbulence. *Boundary-Layer Meteorology*, **3**, 565–587.

Raupach, M., J. Finnigan, and Y. Brunet, 1996: Coherent eddies and turbulence in vegetation canopies: The mixing-layer analogy. *Boundary-Layer Meteorology*, **78 (3)**, 351 – 382.

Ruck, B., and E. Adams, 1991: Fluid mechanical aspects of the pollutant transport to coniferous trees. *Boundary-Layer Meteorology*, **56**, 163– 195.

Ruck, B., and F. Schmitt, 1986: Das strmungsfeld der einzelbaumumstrmung abschtzung von depositionswahrscheinlichkeiten fr feinsttrpfchen. *Forstwissenschaftliches Centralblatt*, **105**, 178– 196.

Salim, M. H., K. H. Schlünzen, and D. Grawe, 2015: Including trees in the numerical simulations of the wind flow in urban areas: Should we care? *Journal of Wind Engineering and Industrial Aerodynamics*, **144**, 84–95.

Singh, B., 2010: Developement of a fast response dispersion model for virtual urban environment. Ph.D. dissertation, University of Utah.

Speckart, S., and E. Pardyjak, 2014: A method for rapidly computing windbreak flow field variables. *Journal of Wind Engineering and Industrial Aerodynamics*, **132**, 101 – 108.

Taylor, P. A., and J. R. Salmon, 1993: A model for the correction of surface wind data for sheltering by upwind obstacles. *Journal of Applied Meteorology*, **32 (11)**, 1683–1694.

Xiao, Q., E. G. McPherson, J. R. Simpson, and S. L. Ustin, 1998: Rainfall interception by sacramento's urban forest. *Journal of Arboriculture*, **24**, 235–244.

Yamaguchi, A., K. Enoki, and T. Ishihara, 2009: A general canopy model for the wind prediction in the forrest and the urban area. *The Seventh Asia-Pacific Conference on Wind Engineering*.

CHAPTER 2

DESCRIPTIONS OF MODELS

2.1 Modeling in QUIC-URB

QUIC-URB is a fast-response simple CFD wind field modeling system that uses empirical parametrisations along with mass conservation to produce a time-averaged three-dimensional wind field (Singh et al., 2008; Singh, 2010; Brown et al., 2013). These two characteristics allow QUIC-URB to produce three-dimensional wind fields extremely fast in complex urban environments. The model is based on the work of Rockle (1990). QUIC-URB generates a gridded domain and applies the mass conservation in each grid cell along with various empirical algorithms that consider the physics of flow around different urban infrastructure elements such trees, buildings, street canyons, intersections, and parking garages (Singh, 2010). Hence, the methodology starts by applying an initial wind field that is composed of various urban parametrisations ($\vec{V}^o = u^o\hat{i} + v^o\hat{j} + w^o\hat{k}$) and forcing the wind field to be divergence free by minimizing the difference between this initial (or guessed) wind field and a final wind field which conserves mass ($\vec{V} = u\hat{i} + v\hat{j} + w\hat{k}$) (Singh et al., 2008). This is achieved by applying a variational technique introduced by Sasaki (1970) to minimize Eq. 2.1.

$$\begin{aligned} E(u,v,w,\lambda) = \int_V [&\alpha_1^2(u-u^o)^2 + \alpha_1^2(v-v^o)^2 + \alpha_2^2(w-w^o)^2 \\ &+ \lambda(\frac{\partial u}{\partial x} + \frac{\partial v}{\partial y} + \frac{\partial w}{\partial z})]dxdydz \end{aligned} \tag{2.1}$$

In Eq. 2.1, λ is a Lagrangian multiplier and α_i are Gaussian moduli that act as weighting factors (Singh et al., 2008) to correct the velocity components. For most urban cases, $\alpha_i = 1$ produces the best results. The final wind field is updated by using the Euler-Lagrangian equations shown in Eq. 2.2.

$$
\begin{aligned}
u &= u^o + \frac{1}{2\alpha_1^2}\frac{\partial \lambda}{\partial x} \\
v &= v^o + \frac{1}{2\alpha_1^2}\frac{\partial \lambda}{\partial y} \\
w &= w^o + \frac{1}{2\alpha_2^2}\frac{\partial \lambda}{\partial z}
\end{aligned}
\tag{2.2}
$$

Equation 2.1 is a system of equations subject to boundary conditions at solid surfaces and at inflow/outflow boundaries. In order to solve for the λ field, Eq. 2.2 is differentiated and substituted into the continuity equation. This leads to Poisson's equation shown in Eq. 2.3, which is then solved for λ using a successive over-relaxation (SOR) solver.

$$
\frac{\partial^2 \lambda}{\partial x^2} + \frac{\partial^2 \lambda}{\partial y^2} + \left(\frac{\alpha_1}{\alpha_2}\right)^2 \frac{\partial^2 \lambda}{\partial z^2} = -2\alpha_1^2 \left(\frac{\partial u^o}{\partial x} + \frac{\partial v^o}{\partial y} + \frac{\partial w^o}{\partial z}\right) \tag{2.3}
$$

QUIC-URB relies on empirical parametrisations that are defined based on the geometry of urban elements and the flow characteristics near these geometries. Parts of the domain that are not affected by buildings or vegetation are initialized with an upwind boundary-layer profile that can be specified as a log-law, power-law, or other user-specified profile. These parametrisations can be applied to any arbitrary upwind flow direction.

2.2 Isolated tree wake model

2.2.1 Single-tree flow characteristics

An individual tree plays an important role in flow dynamics in the proximity of vegetation elements. A wake is the region downstream where the wind speed is reduced and possibly recirculated due to the drag force exerted by foliage. Generally, for any type of obstacle (buildings or vegetation) eddies are shed in downwind (Leenders et al., 2007). The larger eddies break up and create smaller eddies and unstable flow in the wake zone. The wake of a building is more predictable since the recirculation always occurs as a result of well-defined separation points and the fact that buildings are rigid. Vegetation wakes can be more complex because they are flexible, porous, and have extremely diverse geometry (Leenders et al., 2007) Judd et al. (1996) categorized the flow around a two-dimensional porous object into six regions shown in Fig. 2.1. Leenders et al. (2007) stated this classification is

appropriate for single vegetation elements. These regions include: (1) incident flow that is not affected by vegetation; (2) a displaced wind profile region due to the mass conservation, where streamlines are shifted vertically; (3) a bleed flow region where air penetrates through the obstacle due its permeability and velocity magnitude is reduced; (4) a quiet zone where minimum wind speed occurs, and depending on morphological features and the incident flow, flow reversal and recirculation can occur; (5) a mixing layer or wake zone on the leeward side of the vegetation where the inflection in wind profile occurs; (6) a re-equilibrium zone where the wind profile approaches the incident flow.

2.2.2 Canopy model

The initial flow field for a vegetative canopy is parameterised in QUIC-URB using a simplified model based on the work of Macdonald (2000) and Cionco (1965) and described in Pardyjak et al. (2008) for wide, horizontally homogeneous canopies (i.e., the horizontal extent of the canopy is much greater that its height) without a wake. The main assumptions for this canopy model are: 1) a uniform vertical leaf area distribution, 2) a uniform vertical drag coefficient, and 3) a drag coefficient that is independent of the local Reynolds number (Cionco, 1965). Above the canopy, it is assumed that the flow can be characterized with the following logarithmically displaced velocity profile

$$u(z) = \frac{u_*}{k}[\ln(\frac{z-d}{z_0}) - \psi(\frac{z-d}{L})]. \tag{2.4}$$

In Eq. 2.4, u_* is the friction velocity, k is the Von-Karman constant (≈0.4), z is vertical coordinate, z_0 is aerodynamic roughness length, d is displacement height, and L is the Monin-Obukhov length scale which is defined by users, and ψ is the stability function (Eq. 2.5) given by Arya (2001) where $\chi = (1 - 15(z/L))^{1/4}$. In QUIC-URB, both u_* and z_0 are acquired from a linear regression of the velocity profile above canopy (Amatul, 2006). Within the canopy, the mean wind profile is exponential and follows a profile based on the work of Cionco (1965) as presented in Eq. 2.6.

$$\begin{aligned}
\psi(z/L) &= -5\frac{z}{L} \qquad z/L \geq 0 \qquad \text{Neutral and stable} \\
\psi(z/L) &= \ln[(\frac{1+\chi^2}{2})(\frac{1+\chi}{2})^2] - 2\tan^{-1}\chi + \frac{\pi}{2} \\
&\qquad z/L < 0 \qquad \text{Unstable}
\end{aligned} \tag{2.5}$$

$$u(z) = u_H \exp[\alpha(\frac{z}{H_{can}} - 1] \tag{2.6}$$

Here, u_H is the wind speed at the top of canopy ($z = H$), α is an attenuation coefficient, and H_{can} is the height of the canopy. In this approach, the velocity and the slope of wind profile are matched at the height of the canopy (H_{can})(Amatul, 2006; Pardyjak et al., 2008). Matching the velocity at the canopy height leads to the following set of equations (Eq. 2.7 and 2.8) where a simple bisection method is applied to solve for d and u_{Hcan}.

$$\frac{H_{can}}{H_{can}-d}\Phi\left(\frac{H_{can}-d}{L}\right) = \alpha\frac{u_H k}{u_*} \tag{2.7}$$

$$u_{Hcan} = \frac{u_*}{k}\ln(\frac{H_{can}-d}{z_0}) - \psi\left(\frac{H_{can}-d}{L}\right) \tag{2.8}$$

Here, Φ is the universal stability function that is given by Arya (2001) and Pardyjak et al. (2008) as:

$$\begin{aligned}
\Phi\left(\frac{z-d}{L}\right) &= 1 + 5\left(\frac{z-d}{L}\right) \qquad z/L \geq 0 \qquad \text{Neutral and stable} \\
\Phi\left(\frac{z-d}{L}\right) &= \left(1 - 15\frac{z-d}{L}\right)^{-1/4} \qquad z/L < 0 \qquad \text{Unstable.}
\end{aligned} \tag{2.9}$$

Amatul (2006) validated this QUIC-URB canopy model against experimental results from Cionco (1965) for a variety of canopy types. This approach works best within the canopy where the effect of bleed flow is only considered and the downstream canopy wake is completely neglected.

2.2.3 Vegetation wake model

While the canopy model described above is reasonable for relatively dense homogeneous canopies, it is not appropriate for isolated or very sparse canopies. For a very sparse canopy, the height and width of the canopy are of the same order and the appropriate model is three dimensional (Leenders et al., 2007). To address situations where isolated trees may play an important role, a new vegetation wake model is developed. The new model has both analytical and empirical features and is based on

the work of Horne (2012) who used large-eddy simulations (LES) to study the impact of an isolated tree on momentum and turbulent transport in the ABL. The model neglects buoyancy effects and has the ability to predict the average flow dynamics around isolated vegetation elements. The model consists of analytical equations for an axisymmetric wake with a nonlinear spread rate (Agrawal and Prasad, 2003). The simplified time-averaged streamwise momentum equation for an axisymmetric wake can be written as

$$U\frac{\partial U}{\partial x} + \frac{1}{r}\frac{\partial r\overline{uu_r}}{\partial r} = 0, \tag{2.10}$$

where the overbar is an ensemble averaging operator, u_r is the velocity in the radial direction, r (measure from the center of the wake, see Fig. 2.1). The velocity fluctuation in the streamwise (x) direction is given by u, U is mean streamwise velocity, and $\overline{uu_r}$ is the Reynolds stress. It is assumed that the radial velocity is much smaller than the streamwise velocity component and, hence, is neglected. Assuming the axisymmetric streamwise velocity defect $u_d(x, y, z)$ has a Gaussian distribution, a three-dimensional solution to Eq. 2.10 may be written as shown Eq. 2.11, suggested by Agrawal and Prasad (2003) and Horne (2012).

$$u_d = u_c \exp\left(\frac{-r^2}{\lambda^2\delta^2}\right) \tag{2.11}$$

Here, $u_c(x)$ is the velocity defect along the centerline of Gaussian profile, δ is the wake radius, and λ is a scaling constant ($\lambda^2 = 0.08$ based on Horne (2012)). The schematic plot of wake parameters is shown in Fig. 2.1. By assuming a Gaussian distribution for the velocity defect (u_d), the streamwise velocity ($\overline{u}$) can be obtained from Eq. 2.12, where u_0 is the inlet streamwise velocity taken at the same height as $\overline{u}$.

$$\overline{u} = u_0 - u_d \tag{2.12}$$

Generally, δ is assumed to depend on x only. However, due to the nonlinear spread rate of wake in the θ direction, the wake width is greater than its height. Therefore, here it is assumed that δ is the function of x and θ. The mathematical formulation for this relationship, suggested by Horne (2012), is given in Eq. 2.13, where h is the tree height and $B(x)$ is a function that describes the streamwise variation of δ and can be obtained from Eq. 2.14 for the near wake ($x/h < 12.77$) and from Eq. 2.15

for the far wake ($x/h > 12.77$). As indicated in the expressions, $B(x)$ is linear in the near-wake region and follows a power-law farther from the tree.

$$\frac{\delta}{h} = 1.15\cos(2\theta) + \frac{B(x)}{h} \tag{2.13}$$

$$\frac{B}{h} = 0.05(\frac{x}{h}) + 2.22 \qquad x/h < 12.77 \tag{2.14}$$

$$\frac{B}{h} = 1.70(\frac{x}{h})^{0.19} \qquad x/h > 12.77 \tag{2.15}$$

u_c and B are approximated similarly. Hence, the near-wake region is a linear function (Eq. 2.16) and the far-wake is a power-law expression (Eq. 2.17).

$$\frac{u_c}{u_*} = -0.63(\frac{x}{h}) + 9.33 \qquad x/h < 12.77 \tag{2.16}$$

$$\frac{u_c}{u_*} = 90.68(\frac{x}{h})^{-1.48} \qquad x/h > 12.77 \tag{2.17}$$

In Eq. 2.13, θ dependency is considered as cosine function where amplitude is determined from extreme cases for $\theta = 0, \pi/2$. Considering an arbitrary $y - z$ plane downstream of a tree, here increasing θ in range of $[\pi/4, \pi/2]$ contributes to decrease in δ . On the other hand, increasing θ in the range of $[\pi/2, 3\pi/4]$ leads to increase in δ, causing the δ to have a nonphysical heart shape for $[\pi/4, 3\pi/4]$ and $[5\pi/4, 7\pi/4]$ at the polar regions. One possible solution is to assume constant value of velocity defect for problematic region.

2.3 Implementation of a vegetation wake model in QUIC-URB

The numerical approach is implemented as follows: 1) QUIC-URB initializes the velocity at all grid cells in the domain using user-defined profiles and reference values, 2) proper sub-domains in regions downwind of vegetation elements are defined as a wake zone based on tree geometry, 3) the Cionco model is used to specify velocities inside individual tree crowns as an initial wind field, 5) the wake model is applied in defined region by specifying a Gaussian distribution as an initial wind profile, 6) the entire flow field is forced to conserve mass following the procedure described in section 2.1 find the final wind field. Note that the method has been adapted so that the model can handle incident winds from arbitrary angles.

In Chapter 3, we present results validating QUIC-URB against published wind-tunnel experiments. In Chapter 4, the new model is tested at full scale using a field experiment conducted at the University of Utah.

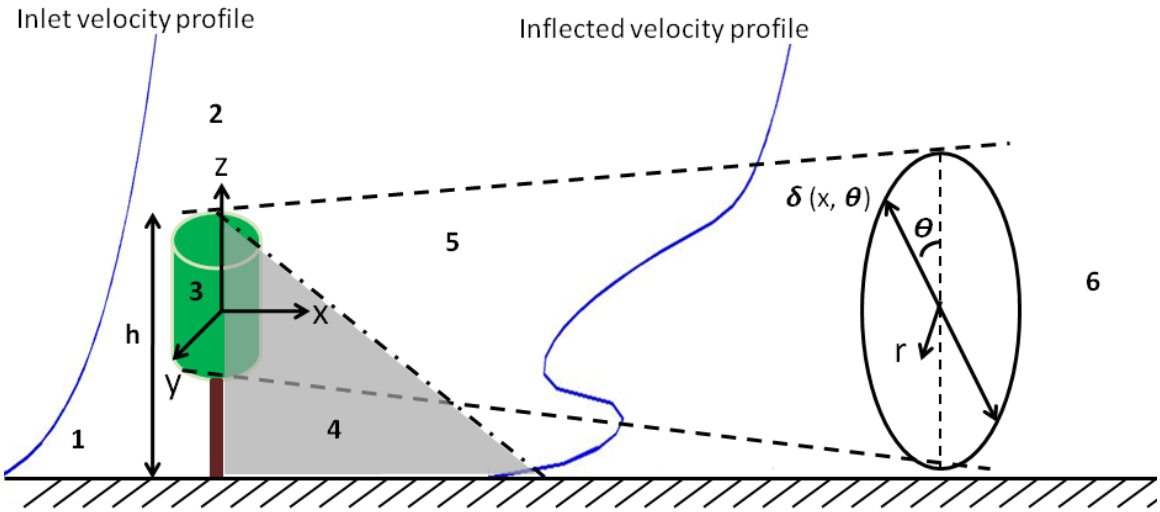

Figure 2.1. Schematic of idealized tree and axisymmetric wake parameters for the vegetation wake model. Note that the wind is assumed to be blowing from left to right in the figure. Numbers show: 1) Incident flow, 2) Displaced flow, 3) Bleed flow, 4) Quiet zone, 5) Mixing zone, and 6) Re-equilibrium zone.

2.4 References

Agrawal, A., and A. K. Prasad, 2003: Integral solution for the mean flow profiles of turbulent jets, plumes, and wakes. *Journal of Fluids Engineering*, **125 (5)**, 813 – 822.

Amatul, U., 2006: Implementation and validation of particle transport model for vegetation in QUIC Urban dispersion modelling system. Master thesis, University of Utah.

Arya, S., 2001: Introduction to microclimeteorology. *second edition Academic Press*, 420.

Brown, M. J., A. A. Gowardhan, M. A. Nelson, M. D. Williams, and E. R. Pardyjak, 2013: QUIC transport and dispersion modelling of two releases from the joint urban 2003 field experiment. *International Journal of Environment and Pollution*, **52 (3-4)**, 263–287.

Cionco, R. M., 1965: A mathematical model for air flow in a vegetative canopy. *Journal of Applied Meteorology*, **4 (4)**, 517–522.

Horne, W., 2012: Flow around a solitary tree in a large field under neutral atmospheric stratification. Master thesis, University of Utah.

Judd, M., M. Raupach, and J. Finnigan, 1996: A wind tunnel study of turbulent flow around single and multiple windbreaks, part 1: velocity fields. *Boundary-Layer Meteorology*, **80 (1)**, 127 – 165.

Leenders, J., J. Van Boxel, and G. Sterk, 2007: The effect of single vegetation elements on wind speed and sediment transport in the sahelian zone of Burkina Faso. *Earth Surface Process and Landforms*, **32**, 1454– 1474.

Macdonald, R., 2000: Modelling the mean velocity profile in the urban canopy layer. *Boundary-Layer Meteorology*, **97**, 25–45.

Pardyjak, E., S. Speckart, F. Yin, and J. Veranth, 2008: Near source deposition of vehicle generated fugitive dust on vegetation and buildings: Model development and theory. *Atmospheric Environment*, **42 (26)**, 6442 – 6452.

Rockle, R., 1990: Bestimmung der stromungsverhaltnisse im bereich komplexer bebauungsstrukturen. Ph.D. dissertation, der Technischen Hochschule Darmstadt.

Sasaki, Y., 1970: Some basic formalisms in numerical variation analysis. *Monthly weather review*, **98 (12)**, 875 –883.

Singh, B., 2010: Developement of a fast response dispersion model for virtual urban environment. Ph.D. dissertation, University of Utah.

Singh, B., B. Hansen, M. Brown, and E. Pardyjak, 2008: Evaluation of the QUIC-URB fast-response urban wind model for a cubical building array and wind building street canyon. *Environmental Fluid Mechanics*, **8**, 281– 312.

CHAPTER 3

VALIDATION OF THE VEGETATION WAKE MODEL

3.1 Setup

In order to validate the canopy wake model, it is critical to find wind-tunnel studies that have been conducted on an isolated tree. To the authors' knowledge, there were only two such studies. These studies formed the basis for the validation presented below. The first is a particle image velocimetry (PIV) wind-tunnel study that was carried out by Lee et al. (2014) to investigate the shelter effect of a real fir tree for two different optical porosities. Two experimental cases were included; one was for a tree with leaves and the other was a leafless case. The inlet flow was well represented by a power-law profile with an exponent of $n = 0.16$. Wind profile data were acquired at ten locations downstream of the tree. Table 3.1 provides detailed test case information used in the QUIC-URB validation simulations. To determine leaf area index (LAI) from optical porosity, Guan et al. (2003) suggested an empirical relation shown in Eq. 3.1, where α is aerodynamic porosity and β is optical porosity. Another approach for calculating optical porosity is to use Beer's law formulation (Martens et al., 1993), as shown in Eq. 3.2, which for a uniform canopy, γ can be approximated by Eq. 3.3. Using this relationship, we can facilitate the comparison of results among different experiments that quantify vegetation density differently. The second study is a wind-tunnel investigation by Ohahsi (2004) of flow around an isolated deciduous tree with known leaf area density. The inlet streamwise velocities were measured at four different heights. Wind profiles were used at three downstream locations. Table 3.1 presents the setup for this test case used in the QUIC validation.

$$\alpha = \beta^{0.4} \tag{3.1}$$

$$\beta = \exp(-\gamma W) \tag{3.2}$$

$$\gamma = \frac{LAI}{H} \tag{3.3}$$

To validate the canopy wake model, wind profiles from these experimental studies are compared against QUIC-URB. Grid resolution and the geometric configuration of the trees modeled in this study are presented in Table 3.2. Since the horizontal grid resolution is larger than a typical trunk diameter (0.6 m), aerodynamic effects associated with the trunk are neglected and the Gaussian wake wind profile is shifted in the vertical direction based on trunk height. Inlet profiles in QUIC were specified based on the profiles given in Lee et al. (2014) and Ohahsi (2004). Table 3.3 provides flow properties at the reference height and inlet profile features (u_* and z_0) that were obtained by regression analysis of the experimental data.

3.2 Results of the wake model

3.2.1 QUIC-URB qualitative results

Figure 3.1 shows results from a QUIC-URB simulation with the vegetation wake model for a simple tree case with a logarithmic inlet profile and a wind direction in $+x$ direction. Normalize velocity magnitude contour plots are shown at four x locations downstream of the tree. A modified version of the QUIC-URB vegetation wake model with this explanation is shown in Fig. 3.2. As it is shown, this modification resolved the polar points problem. In general, as a result of drag force on the tree, immediately downstream of the tree, the flow decelerates. The height that maximum deceleration occurs is at the height of maximum LAD for typical deciduous trees ($z = 0.7h$). The velocity deficit decreases downstream as a zone of re-equilibrium is approached and the upwind profile is re-established. The flow physics in the wake zone are similar to the effect of a windbreak, where the mean streamwise velocity profile has an inflection point and then approaches the inlet profile far downstream. However, unlike traditional windbreak models, the geometry and the model are fully three dimensional because of the Gaussian distribution used to parameterise the velocity deficit.

Contour plots of the normalized mean spanwise velocity at two locations downstream of the tree, $1.5h$ and $4h$, are shown in Figure 3.3. Two regions of flow

acceleration can be observed. In QUIC-URB, the streamwise velocity is obtained from the wake model and the other velocity components are determined from mass conservation. Therefore, these corresponding acceleration regions tend to bring fluid into the wake zone. Figure 3.4 shows contour plots of the normalized mean vertical velocity component at two locations downstream of the tree, $1.5h$ and $4h$. Similar pattern as the spanwise direction is observed where vertical velocity tend to bring more flow to the wake due to the loss of momentum in the presence of the tree. Vertical velocity is in the same order as the spanwise velocity and both are much smaller than the streamwise velocity.

Figure 3.5 depicts the computed normalized velocity magnitude in the $X - Z$ plane along the centerline ($y = 0$) of the tree with an $Y - Z$ plane at $x = 3h$ of the tree. The tree location is shown with the arrow. As discussed in the description of the model, the bleed flow within the canopy follows a Cionco profile. The 3D wake model is invoked immediately after tree nodes and extended to a predefined wake length downstream of tree (here is $4h$). The width of the wake increases moving downstream from the tree and the deficit decreases until the upstream wind profile is recovered. For validation, these simulation results are compared with wind-tunnel data presented by Lee et al. (2014) and Ohahsi (2004).

3.2.2 Quantitative evaluation of vegetation wake model for wind-tunnel test cases

Figures 3.6 and 3.7 show a comparison between QUIC-URB and wind-tunnel data for Case 1 (Lee et al., 2014) at eight different downstream locations and statistical metrics, respectively. The statistical metrics of fractional bias (FB), mean error, normalized absolute difference (NAD), and absolute difference (AD) are applied in this work since they are the error metrics considered in many other studies in this area (Gowardhan et al., 2011; Neophytou et al., 2011). These metrics are calculated using Eqs. 3.4 to 3.7, where n is the total number of experimental locations, and E and S indicate experimental and simulation results, respectively.

$$\mathrm{FB} = \frac{\overline{S} - \overline{E}}{0.5(\overline{E} + \overline{S})} \tag{3.4}$$

$$\text{Mean Error} = \sum_{i}^{n} \frac{|E(i) - S(i)|}{n} \tag{3.5}$$

$$\text{Normalized Absolute Difference} = \frac{\sum_{i}^{n} |E(i) - S(i)|}{\sum_{i}^{n} [E(i) + S(i)]} \tag{3.6}$$

$$\text{Absolute Difference} = \frac{\sum_{i}^{n} |E(i) - S(i)|}{n} \tag{3.7}$$

Qualitative comparison of the streamwsie velocity for these eight locations is shown in Fig. 3.6, where the result indicates that the QUIC-URB wake model agrees well with experimental data. The leafless case shows better agreement at all downstream locations, with less than 15% relative error. However, for the control case, the relative error immediately downstream of the tree (at x/h = 1) shows more than 100% difference. Farther downstream, the error decreases; at $x/h > 2$ relative errors for all conditions are less than 15%. The Fractional Bias (FB) is also shown in the statistical metrics plot, which indicates substantial underestimation of the velocity deficit for $x/h < 2$. This might be due to inadequate knowledge about the flow in close proximity of the tree. Specifically, the flow in the quiet zone may or may not recirculate. In the control case, because of a large LAI, a recirculation zone is observed in the data for $x/h \leq 2$. Previous studies simulated and observed the existence of a recirculation zone leeward of forest clearings. Cleugh (1998), Wang and Takle (1995), Frank and Ruck (2008), and Lee and Lee (2012) observed a triangular shaped zone that is bounded by a forest, or windbreak and the ground with a line that is formed starting from top of the most downstream trees and intersecting the ground at $3H$-$8H$ (shown in Fig. 2.1). The dimensions of the recirculation zone are influenced by the approaching flow and canopy morphology. In general, for a dense shelterbelt with a porosity of less than 0.3, a recirculation zone is reported in the literature. Hence, the wake parametrisation implemented in QUIC-URB needs to be interpreted with caution in the quiet zone and in the the recirculation zone. To address the effects of LAI on the QUIC-URB vegetation wake model with respect to the Lee et al. (2014) results, normalized velocities along the tree centerline at $z = 0.7h$ (the height of maximum LAD) are shown in Fig. 3.8. As expected (based on Eq. 2.16), the centerline velocity for QUIC-URB has a gentle linear trend. The same linear feature is observed for the leafless data. In contrast, the control condition (deciduous

tree) has an exponential increase for ($x/h < 2$) and a linear trend afterward. Since the wake parametrisation includes this centerline velocity in its calculation, these deviations likely cause the large differences observed between QUIC-URB and the control condition just downwind of the tree.

Figure 3.9 shows normalized streamwise velocities for Case 2 (Ohahsi, 2004) at three downstream locations (x/h=1,2, and 3) in the bleed-flow zone. Figure 3.9 (a) shows the inlet profiles for QUIC-URB and the data of Ohahsi (2004). Clearly, the profiles do not match well and the 3.9 profile is not a standard logarithmic profile. We hypothesize that the discrepancy observed in the inlet profiles is a result of the experimental data being reported too close to the tree. That is, the inlet profile was measured at $x/h = -0.5$ where the presence of the tree likely changed the mean flow. Moreover, the measurements were made very close to the wind-tunnel inlet, which could also cause deviations from an equilibrium boundary-layer flow. Hence, to best approximate the 'effective' upstream wind profile, a logarithmic profile was specified based on a best-fit to the flow above and downstream of the tree. The mean wind profiles show good agreement for all locations (< 30% relative error). Unlike Case 1, the vegetation wake model has reasonable agreement immediately downwind of the tree. This might be due to better representation of the tree's morphological features in QUIC (compared to the previous case) and the nature of the flow in the near wake for this test case, where the wake is weaker. Statistical metrics for this test case are shown in Fig. 3.10. The absolute difference at all locations is < 0.3 ms^{-1}, and farther downstream, the FB indicates overestimation in the model. This might be partially due to the extrapolation of the Ohahsi (2004) data to compare at $x/h = 3$ since the original paper only presented observations at $x/h = 1, 2, 2.2$. In general, the vegetation wake model seems to have a reasonable accuracy for typical deciduous trees with LAIs < 3.3 and underestimates streamwise velocities for LAI > 3.3 for $x/h < 2$.

Table 3.1. Tree morphological parameters for Case 1: Lee et al. (2014) and Case 2: Ohahsi (2004)

Case	Type	Optical porosity	Calculated LAI	Tree height	Trunk height
1	Control	0.059	4.88	0.19 m	0
1	Leafless	0.79	0.4	0.19 m	0
2	Control	0.19	3.303	0.6 m	0.2 m

Table 3.2. QUIC-URB setup parameters for all simulations

Domain size	Horizontal resolution	Vertical resolution	Tree height	Trunk height	D_{crown}
100m × 100m × 40m	1 m	1 m	20 m	6 m	12 m

Table 3.3. QUIC-URB initial/inlet boundary-layer parameters for all simulations

u_*	z_o	u_{ref}	z_{ref}	Wake Length
0.256 ms^{-1}	0.01 m	5.53 ms^{-1}	50m	$11h$

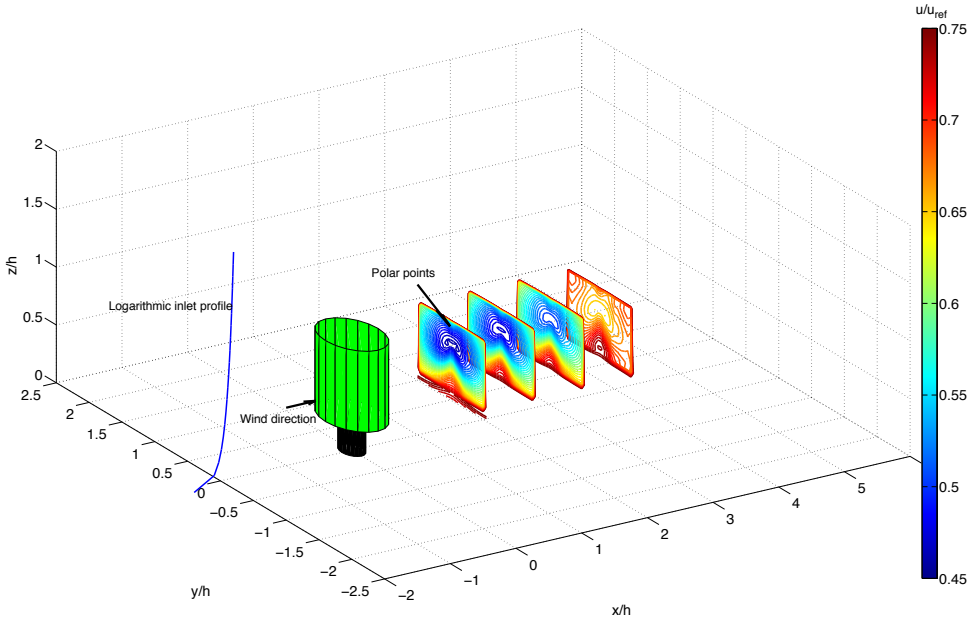

Figure 3.1. Contours of nondimensional velocity magnitude at four locations (x/h=1.5, 2.25,3, and 3.75) downstream of an isolated tree

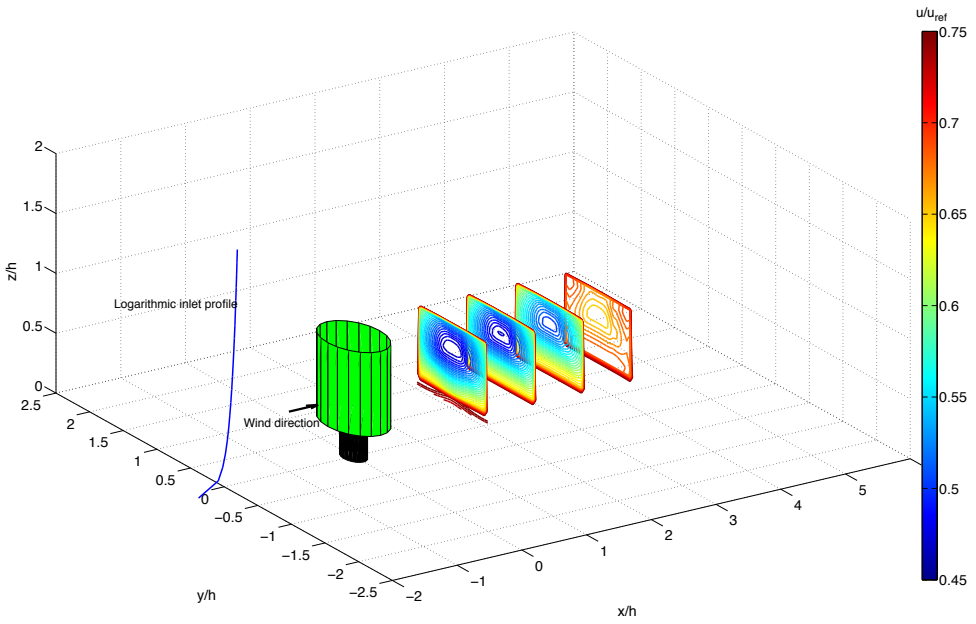

Figure 3.2. Contours of nondimensional velocity magnitude at four locations (x/h=1.5, 2.25,3, and 3.75) downstream of an isolated tree using the improved wake model parameterisation

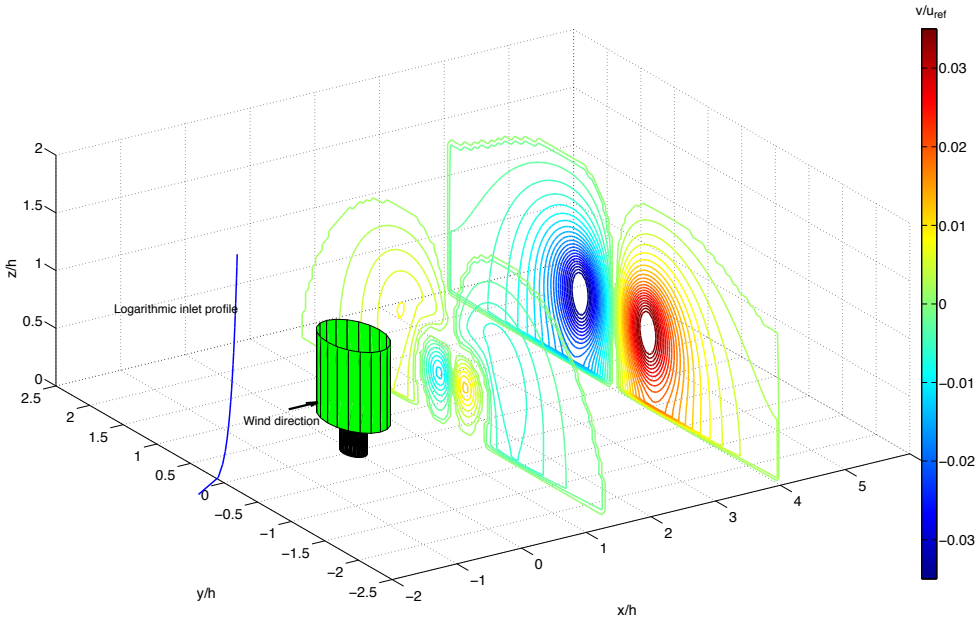

Figure 3.3. Contours of nondimensional spanwise velocity component at two locations (x/h=1.5 and 4) downstream of an isolated tree

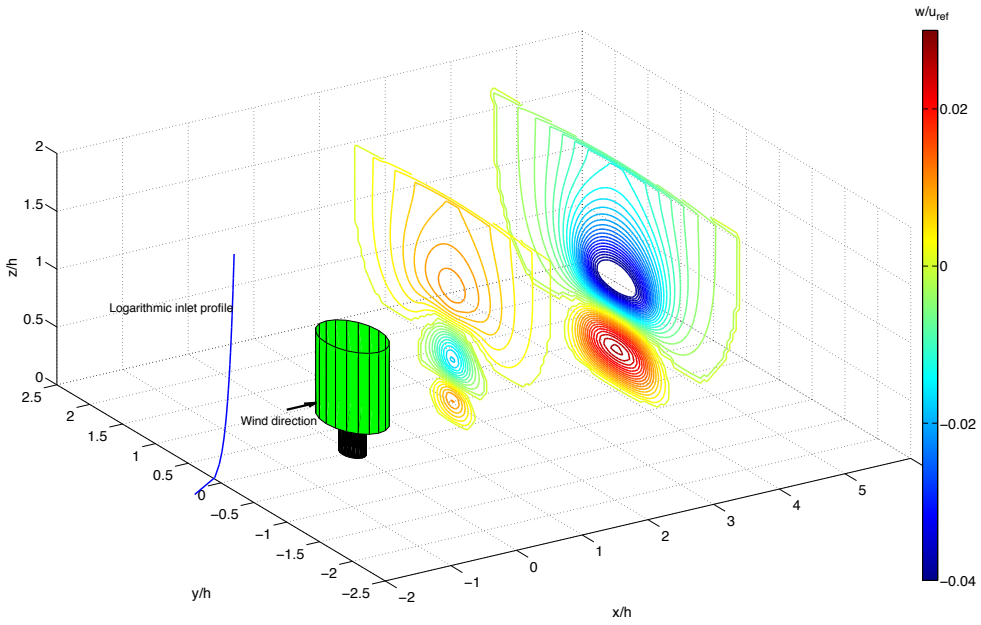

Figure 3.4. Controus of nondimensional vertical velocity at two locations (x/h=1.5 and 4) downstream of an isolated tree

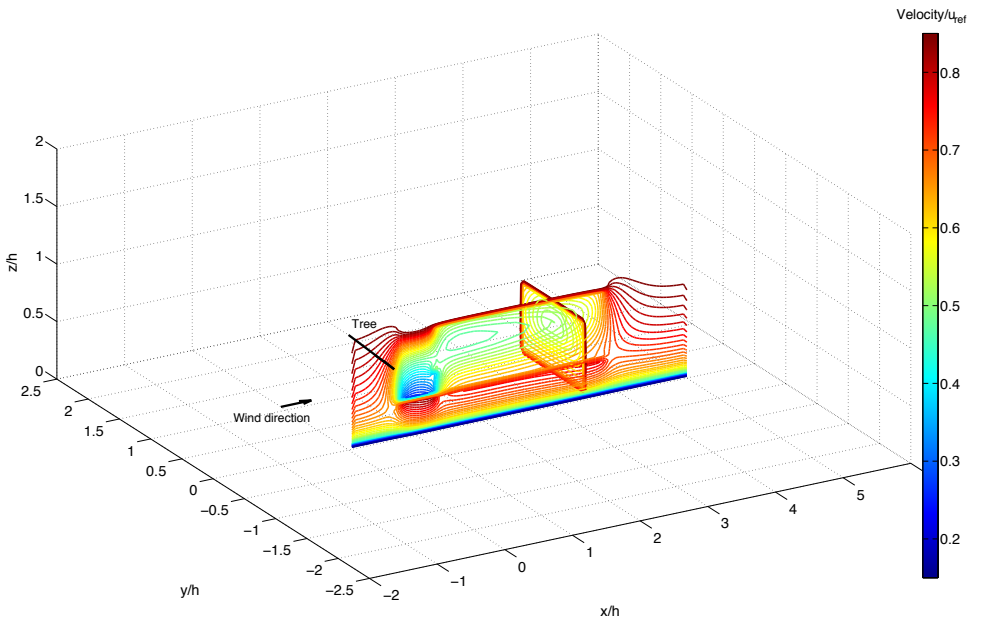

Figure 3.5. Contours of nondimensional velocity in two different planes: an x-z plane taken along the centerline of the tree and a y-z plane taken at x/h = 3

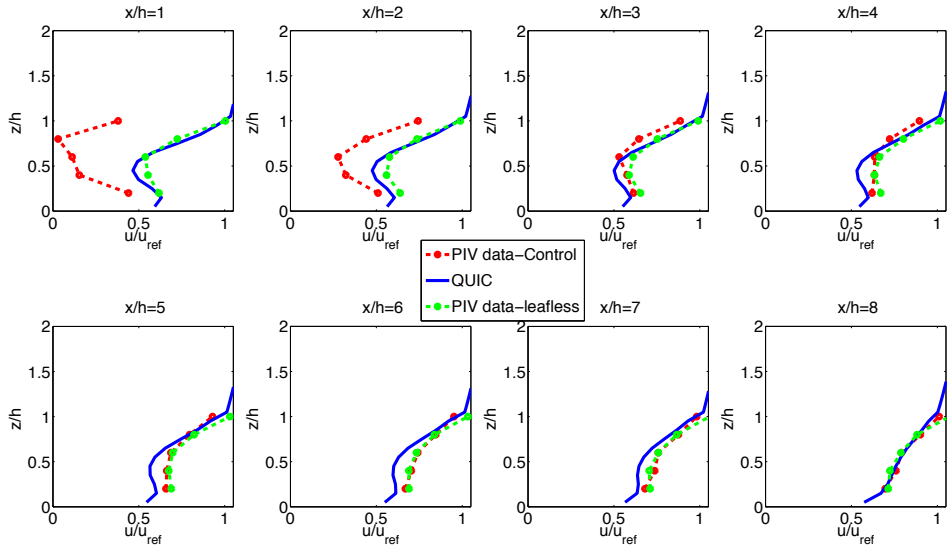

Figure 3.6. Comparison of PIV data (Case 1 in Table 3.1) and QUIC-URB at eight locations downstream (x/h=1 to 8) of the tree for a case with leaves (Control) and without leaves (leafless)

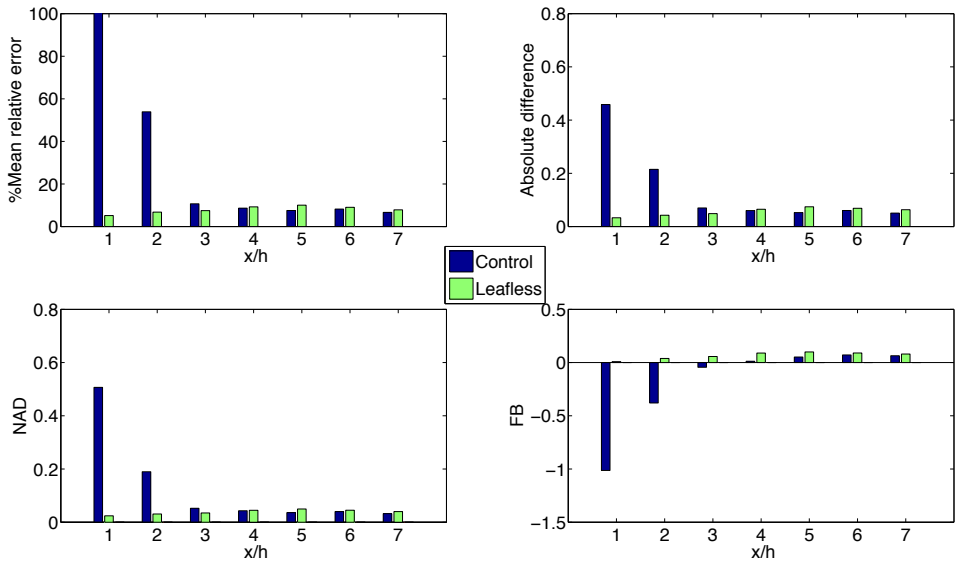

Figure 3.7. Statistical metrics comparing Lee et al. (2014) and QUIC-URB (Case 1 in Table 3.1)

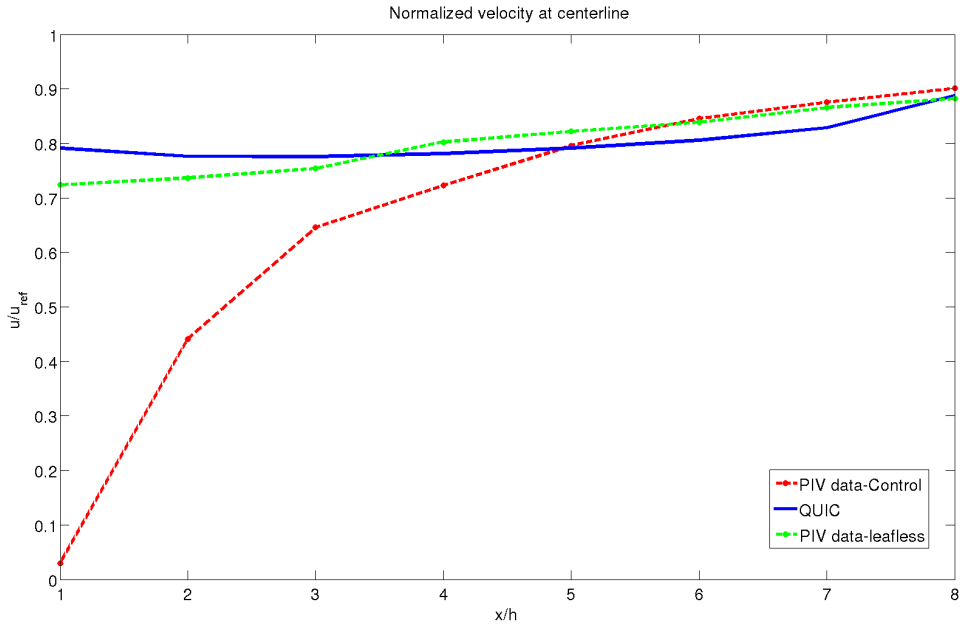

Figure 3.8. Comparison of normalized streamwise PIV and QUIC-URB vegetation wake model streamwise velocities along the centerline ($z/h = 0.7$)

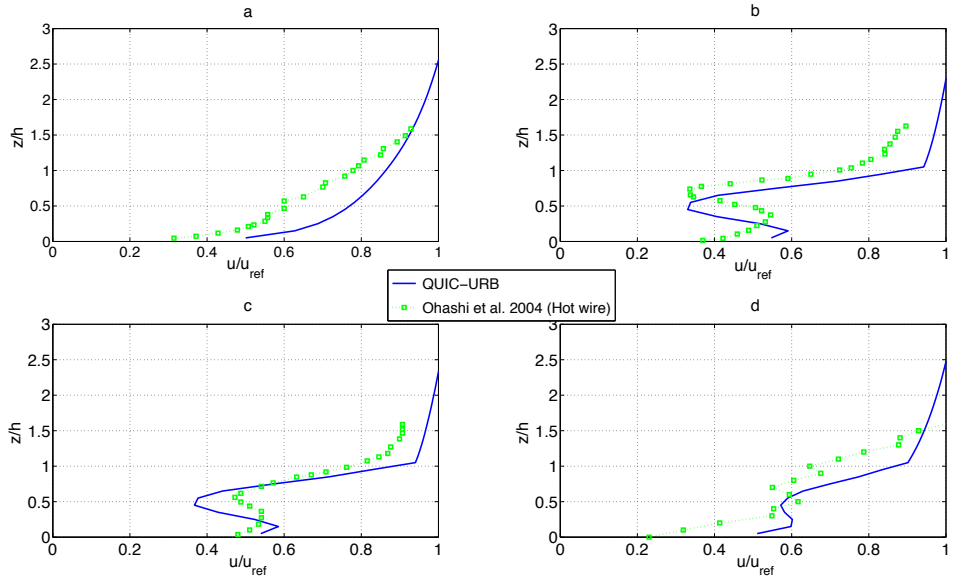

Figure 3.9. Comparison of wind-tunnel data Ohahsi (2004) and QUIC-URB (Case 2 in Table 3.1) at a) the inlet, b) $x/h = 1$, c) $x/h = 2$, and d) $x/h = 3$

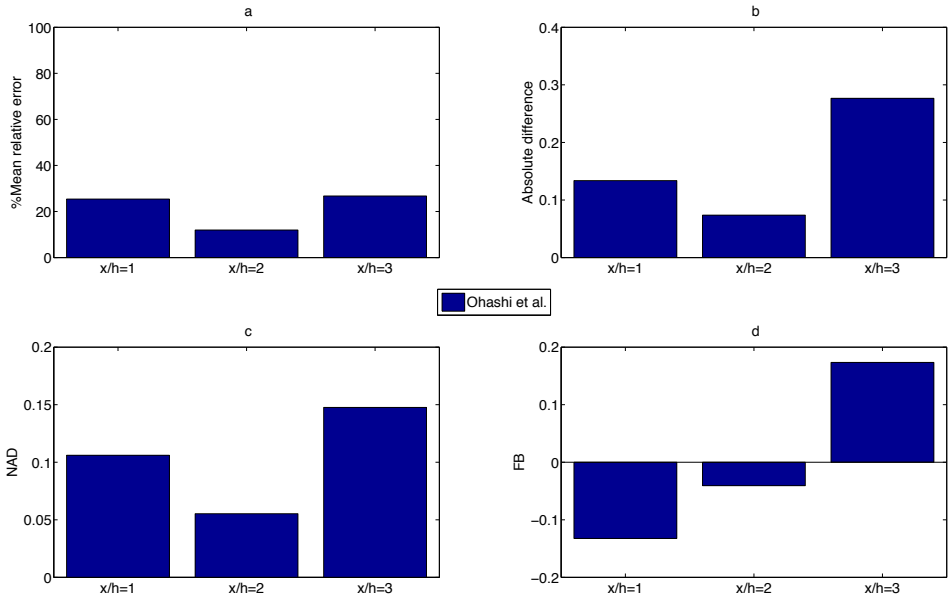

Figure 3.10. Error quantification statistics at $x/h = 1$, $x/h = 2$, and $x/h = 3$ comparing Ohahsi (2004) and QUIC-URB (Case 2 in Table 3.1)

3.3 References

Cleugh, H. A., 1998: Effects of windbreaks on airflow, microclimates and crop yields. *Agroforestry Systems*, **41 (1)**, 55–84.

Frank, C., and B. Ruck, 2008: Numerical study of the airflow over forest clearings. *Forestry: An International Journal of Forest Research*, **81 (3)**, 259.

Gowardhan, A. A., E. R. Pardyjak, I. Senocak, and M. J. Brown, 2011: A cfd-based wind solver for an urban fast response transport and dispersion model. *Environmental Fluid Mechanics*, **11 (5)**, 439–464.

Guan, D., Y. Zhang, and T. Zhu, 2003: A wind-tunnel study of windbreak drag. *Agricultural and Forest Meteorology*, **118 (12)**, 75 – 84.

Lee, J., and S. Lee, 2012: PIV analysis of the bottom gap effect on the flow around a fir tree. *15th International Symposium on Flow Visualization*.

Lee, J.-P., E.-J. Lee, and S.-J. Lee, 2014: Shelter effect of a fir tree with different porosities. *Journal of Mechanical Science and Technology*, **28 (2)**, 565–572.

Martens, S. N., S. L. Ustin, and R. A. Rousseau, 1993: Estimation of tree canopy leaf area index by gap fraction analysis. *Forest Ecology and Management*, **61 (1)**, 91 – 108.

Neophytou, M., A. Gowardhan, and M. Brown, 2011: An inter-comparison of three urban wind models using Oklahoma City joint urban 2003 wind field measurements. *Journal of Wind Engineering and Industrial Aerodynamics*, **99 (4)**, 357 – 368, the Fifth International Symposium on Computational Wind Engineering.

Ohahsi, M., 2004: A study on analysis of airflow around an individual tree. *Journal of Environmental Engineering*, **578**, 91– 96.

Wang, H., and E. S. Takle, 1995: A numerical simulation of boundary-layer flows near shelterbelts. *Boundary-Layer Meteorology*, **75 (1)**, 141–173.

CHAPTER 4

EVALUATION OF QUIC-URB

4.1 Field experiment setup

Wind measurements were carried out during a field experiment conducted at the University of Utah to validate the model at full-scale and to provide insight for future improvements to QUIC-URB (see Figure 4.1). This is an ongoing experiment that started in Summer 2015. During this experiment, low-cost local energy-budget measurement stations (LEMS) (Gunawardena et al., 2017) were deployed throughout the campus (40°45′52.9″N, 111°50′56.9″ W) to acquire continuous measurement of the near-surface time-averaged weather data. The campus site is a region of highly vegetated complex terrain populated mainly by deciduous 75% (200 trees) and coniferous 25% (65 trees) trees, as well as numerous buildings. Figure 4.1 shows 11 locations of the LEMS.

LEMS are custom-built weather stations (see Fig. 4.2) that make use of Arduino Mega 2560 microcontrollers to collect wind speed and direction data using Davis cup and vane anemometers, Sensirion SHT 15 to measure humidity and air temperature, Zytemp TN9 sensors for surface temperature, Licor LI200 sensors for global radiation, and Decagon 5TM sensors for soil moisture and temperature measurements. All sensors were sampled at a frequency of 0.1 Hz. The anemometers were mounted at 2 m above ground. The LEMS were powered with 6 Volt sealed lead-acid batteries paired with 5.2 Watt-8 Volt Sparkfun solar panels. All data are stored on a SD card for each LEMS. LEMS Locations were selected to cover wide variety of urban conditions including: a street canyon (LEMS K), a building wake (LEMS M), and a vegetated canopy (LEMS Q).

Although the LEMS operated most of the time, there were gaps. This is mainly

due to winter storms, battery problems that shut off the microcontroller, and low-wind speeds causing uncertainty in measurements. Gunawardena et al. (2017) evaluated the LEMS by comparing wind speed measurements against high-quality sonic anemometer measurements and found relatively good agreement for wind speeds above 0.5 ms^{-1}. In addition, two specific time periods were selected for comparison when most of the LEMS were in operation, and a high-quality campus weather station showed relatively high wind speeds covering most directions. The test cases are included in Table 4.1.

4.2 University of Utah QUIC-URB simulation details

Figure 4.3 shows a map of the campus test case with the locations of all the LEMS. The white regions around the background map represent a buffer zone that was added to eliminate boundary condition issues that result from building that are too close to the domain edge. Grid resolution was determined by comparing differences between QUIC-URB and the experimental results and finding a threshold where the differences were minimized. For this purpose, results from two grid resolutions were compared and are shown in Table 4.2. The same concept was applied for time averaging period and normalized absolute difference was compared to find the optimum time period as shown in Table 4.2.

QUIC-URB was run with uniform horizontal grid resolutions of 4 m and a vertical resolution of 1.1 m. Details of the simulation domain and grid are shown in Table 4.3. A logarithmic inlet profile (Eq. 4.1) is specified using in QUIC-URB for initial and inlet wind profiles using wind speed and direction U_{ref} at the reference height z_{ref}. z_o in Eq. 4.1 is the aerodynamic roughness length that is assumed to be constant for entire domain and has a typical value of 0.1 m for urban areas (C.S.B. Grimmond, 1998). L in Eq. 4.1 is the Monin-Obukhov length scale that describes the effect of buoyancy in flow regime. For neutral conditions, L is considered to be infinite, and ψ is the stability function (Eq. 2.5). Reference values for wind speed and direction were obtained from MesoWest (MesoWest, 2017). Table 4.4 shows detailed information of reference weather data during the simulation period taken from the William Browning Building (WBB), shown in Fig. 4.1.

$$U(z) = \frac{U_{ref}(\ln((z + z_o)/z_o) + \psi_M(z/L))}{\ln((z_{ref} + z_o)/z_o)} \tag{4.1}$$

4.3 Results and discussion

The results presented below focus on the center of the engineering-quad domain at the University of Utah. The computational domain has been extended by 50 m on all sides to avoid problems that occur when buildings are to close to the edge of the domain. Preliminary simulations results confirm that buffer zone (shown in Fig. 4.3) does not have a significant impact on flow field in the domain. However, further experimental investigations are necessary to verify this. Note that flow in the buffer region is not shown in the results. Our comparison study was focused on several different zones such as: open area, street canyon, building wake, upwind cavity, canopy, and tree wake. The main objective of this section is to qualitatively and quantitatively evaluate QUIC-URB against real-world experimental data for two test cases where vegetation is assumed *a priori* to be important. This study is the first field-scale evaluation of QUIC-URB's vegetation models in a real urban domain.

4.3.1 Qualitative comparison

Figure 4.4 shows qualitative results of the new QUIC-URB vegetation model from Case A taken on 19 March 2017 at 14:30 for a plane at 1.65 m above ground, where the results can be compared with LEMS measurements. The buffer region is eliminated in figures. The vector plots show that QUIC-URB agrees qualitatively with the experimental measurements and that the model simulates wind speed and direction well in open areas of the domain. For this specific time step, the inlet winds are southerly and relatively strong (4 ms^{-1} at the reference). The impact of the trees can be seen particularly well in the region $150 < X < 275$ and $150 < Y < 350$, where the wind speed is reduced and distorted around the trees. As shown in Fig. 4.4 (a), at LEMS F, M, N, and I locations, QUIC-URB underestimates the flow in the upwind cavity zone and side wall. Figure 4.4 (b) is a contour plot of velocity magnitude with overlaid streamlines. Low wind speeds in building wakes are indicated by a dark blue color. Light blue regions in the lee of trees represent wind speed reductions due to tree drag. The red shaded regions in the trees are under the crown and show the

under canopy acceleration due to the mass conservation. Figure 4.5 illustrates the differences between the vegetation wake model and the original QUIC-URB vegetation (Cionco model). Figure 4.5 shows the difference in velocity magnitude between the two models at each grid point. Clearly, the major differences are around trees where the dark blue regions indicate wind speed reductions caused by the presence of the wake. The red zones are regions under the crown where the flow accelerates due to the mass conservation.

Figure 4.6 shows results for a time period during Case B. The buffer region is eliminated in figures. For this specific time, with northwesterly inflow (shown in Fig 4.6 (b)) and relatively high wind speed (5.6 ms^{-1}at the reference), Fig. 4.6 (a) shows reasonably good agreement between the measured and QUIC-URB modeled wind speeds. Wind directions have an acceptable error within ±90° of the experimental data. At the LEMS K location in which the flow has a street canyon type, the model agrees well with the experimental data for velocity magnitude and direction. At LEMS I, QUIC-URB underestimates the flow field in building wake. At LEMS Q, the experimental results match with the simulation extremely well for wind speed and direction.

Figure 4.7 shows a selected time (1 July 2017 at 09:30) with relatively light westerly winds (2 ms^{-1} at the reference, shown in Fig. 4.7 (b)). Based on the vector plot (shown in Fig. 4.7 (a)), at LEMS G and A locations, QUIC-URB underestimates the wind field results which might be due to uncertainty in wind measurements at very low wind speeds. At LEMS E, F, K, H, N, Q, and I locations, QUIC-URB agrees well with the LEMS data.

Figure 4.8 and 4.9 show time series of wind speed during Cases A and B, respectively. Figure 4.8 (a) illustrates a relatively good match between the simulation and experimental data at LEMS H location. Figure 4.8 (b) shows time series of data for LEMS K. QUIC-URB results in both subplots are broadly consistent with the major trends of experimental data. However, at LEMS K, QUIC-URB clearly underestimates wind speeds for the high wind speed case.

Figure 4.9 shows Case B data with a clear diurnal cycle in the wind speed. Figure 4.9 (a) shows the LEMS G location time series which indicates a significant

underestimation in the modeled wind speed. A possible explanation for this error is that LEMS G is located in a building wake and that QUIC-URB underestimates the wake velocity at this location. This is consistent with previous QUIC-URB findings in the literature (Gowardhan et al., 2011; Neophytou et al., 2011; Girard et al., 2017). In contrast to LEMS G, the QUIC-URB results shown in Fig. 4.9 (b) at LEMS I location are in very good agreement with the experimental data, indicating good performance far from buildings.

In general, for both cases (A:19-28 March 2017, B: 29 June to 7 July 2015) qualitative representation of results suggested good agreement of QUIC-URB and experimental results. However, in sub-domains including vegetation, upwind zone, and side wall, QUIC-URB underestimates wind speeds.

4.3.2 Quantitative comparison

In this section, a quantitative and statistical evaluation of QUIC-URB is presented using LEMS data. The goal of this section is to quantify simulated and observed differences in wind speed and wind direction.

For more comparison of wind speed and direction results, wind roses are presented for several locations. A wind rose is a useful graphic that shows distributions of wind speed and wind direction for a specific location. Experimental and simulation wind roses at LEMS locations are presented in Figs. 4.10 to 4.11. Figure 4.10 (a) shows that QUIC-URB slightly underestimates for southwest and overestimates for northwest wind direction. This is in agreement with the results shown in Fig. 4.8. Figure 4.10 (b) shows that QUIC-URB underestimates the frequency and magnitude of southwesterly winds, whereas other wind directions show better agreement with the experimental data. A possible explanation for the discrepancy is that for southwesterly winds, LEMS I might be located in an upwind cavity that leads to underestimation of wind magnitude. Moreover, during southwesterly winds, LEMS H is located in a vegetation wake where underestimation occurs. LEMS K, as shown in Fig. 4.10 (c), confirms that wind speed underestimation occurs in the street canyon zone. Figure 4.11 (a) clearly shows that QUIC-URB poorly predicts wind direction at LEMS G. LEMS G is located at an intersection with a large building just to the west. The building wake at this

location is very sensitive to small perturbations in the larger scale wind. Figure 4.11 (b) demonstrates good agreement between the simulation and experimental results for the LEMS I location.

The statistical metrics are shown in Figs. 4.12 and 4.13. QUIC-URB simulations have been evaluated by: 1) simulating without any vegetation model, 2) simulating with the new vegetation wake model, and 3) simulating with the original Cionco model. Statistical metrics are presented including: fractional bias (FB), Mean Relative Error, and normalized absolute difference (NAD) for wind speed and wind direction calculated by Eq. 3.4 to 3.7.

Figure 4.12 shows the statistical metrics for Case A. LEMS E and H show major changes in wind speed fractional bias, which shows overestimation in no vegetation to underestimation in wake and Cionco model. LEMS E and H are both located close to the vegetation and wake zone. These results concur in good agreement with the qualitative analysis which show slightly underestimation in vegetation wake and Cionco model close to trees. No significant correlation was revealed in mean relative error of three simulation configurations. Figure 4.13 shows the statistical metrics for Case B. LEMS G substantially underestimates wind speeds in all configurations of no trees, wake model, and Cionco model. LEMS A, which is located in a vegetated area, agrees well with the wake model. LEMS N, located very close to a tree, shows overestimation in the wake and no-vegetation model. Despite the limitations of the model, LEMS H, I, M, K, E, and F have good correlations overall. No significant differences of the mean relative error were observed between the no trees, tree wake model, and Cionco model simulations for this test case. A plausible explanation is that the distance of the experimental setup from trees could have influenced the results where no significant differences between the Cionco model and vegetation wake model were observed. Generally, LEMS siting was biased towards locations not having trees as the LEMS have solar charges and would have had problems charging in tree shade.

Figure 4.14 shows wind direction scatter plots for Case A at LEMS A and I locations. The plotted dashed lines show the bounded lines for wind direction error within ±90°. Both Figs. 4.14 (a) and (b) indicate that the model is able to capture major trends and 76% and 71% of the results are within ±90° of the experimental

value, respectively.

Figure 4.15 shows scatter plots comparing observed and computed wind directions at LEMS I and M. The plotted dashed lines show the bounded lines for wind direction error within ±90°. Figure 4.15 (a) and (b) show the model predictions were within 90° of measured data, 77% and 70% of the time, respectively. The data are categorized in two groups: low wind (WS< 2 m/s) and higher wind speeds. This provides a means for better understanding the circumstances leading to better or worse agreement. Figure 4.15 (b) shows the wind direction scatter plot for LEMS M. It is interesting to note that QUIC-URB overestimates wind speeds for easterly winds and underestimates wind speeds for westerly winds, when LEMS M is located in upwind zone. In other words, it can be inferred that the model underestimates wind speeds in building upwind zones and overestimates for cavity zones.

4.4 Computational cost

QUIC-URB is one of the fastest and cheapest CFD methods for complex urban environments. The computational cost for one time step is ≈ 5 sec using a 2.6 GHz MacBook Pro Intel Core i5. There were no significant changes observed in computational cost by adding the vegetation wake model compared to the original QUIC-URB vegetation model. Total computational cost for each Case (A and B) was ≈ 45 minutes on the same computer.

Table 4.1. Selected time period in University of Utah field experiment to compare with QUIC-URB results

Case A	19-28 March 2017	10 days
Case B	29 June to 7 July 2015	9 days

Table 4.2. Grid resolution and time averaging sensitivity study. All simulations were run with a vertical resolution Δz =1.1 m

Case study	Normalize absolute difference
Δx = Δy = 4 m	0.292
Δx = Δy = 3 m	0.265
10 min averaged	0.249
20 min averaged	0.250
30 min averaged	0.239

Table 4.3. QUIC-URB simulation domain specifications

No. Trees	No. Buildings	Averaging time	Horizontal resolution	Vertical resolution	Domain size
210	101	30 min	4 m	1.1 m	600 m × 480 m × 44 m

Table 4.4. MesoWest reference weather station information

Latitude	Longitude	Elevation	Height from ground
40.76	-111.84	1465 m	36 m

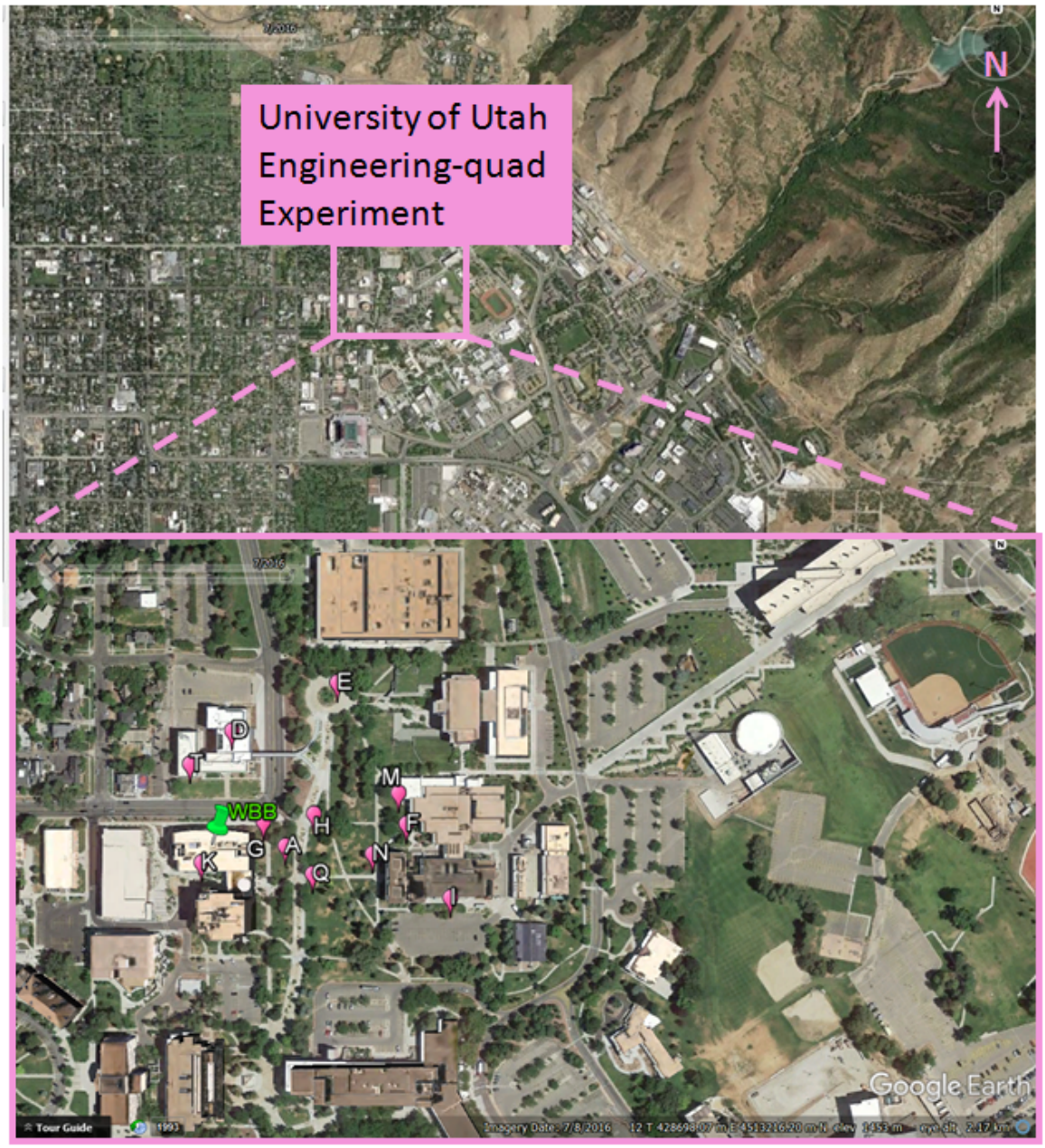

Figure 4.1. Location of the field site at the University of Utah including the 11 LEMS locations and reference weather station at WBB taken from Google Earth (2016)

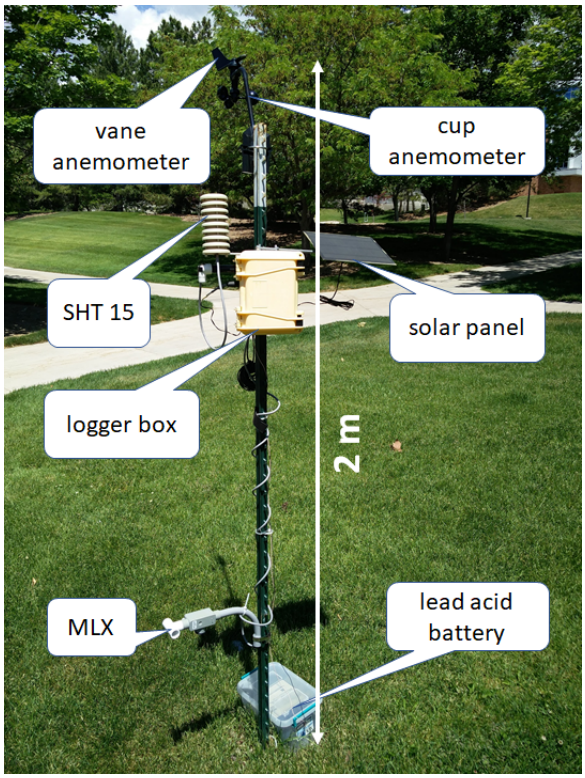

Figure 4.2. Photograph of a typical LEMS configuration

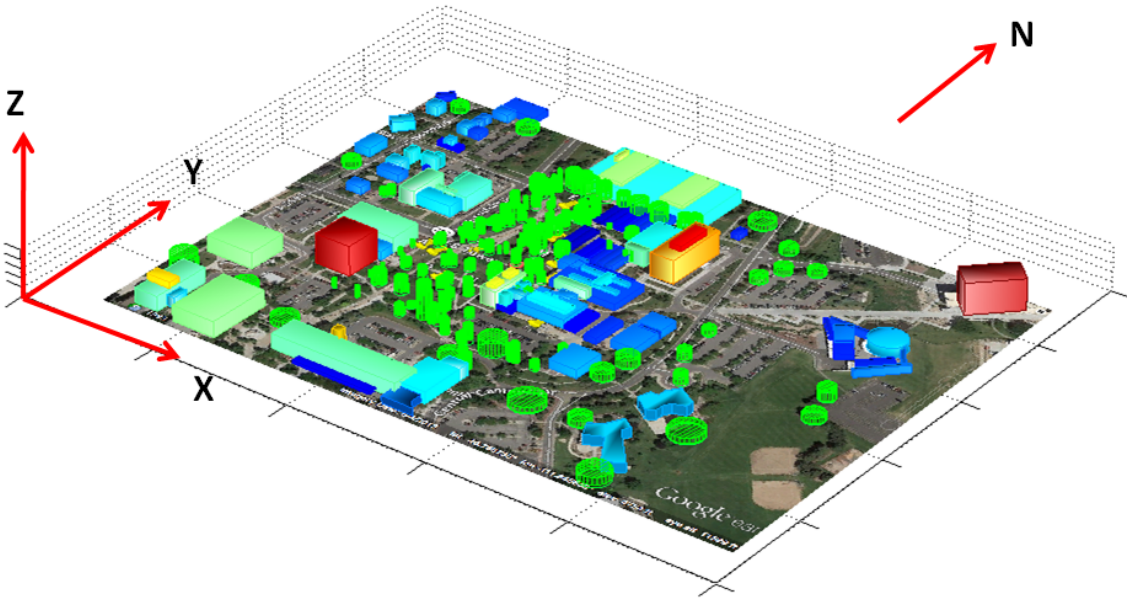

Figure 4.3. QUIC-URB simulation domain. Note that buildings are indicated by filled colors and vegetation is indicated by green translucent cylinders. White regions around the background map are buffer zones.

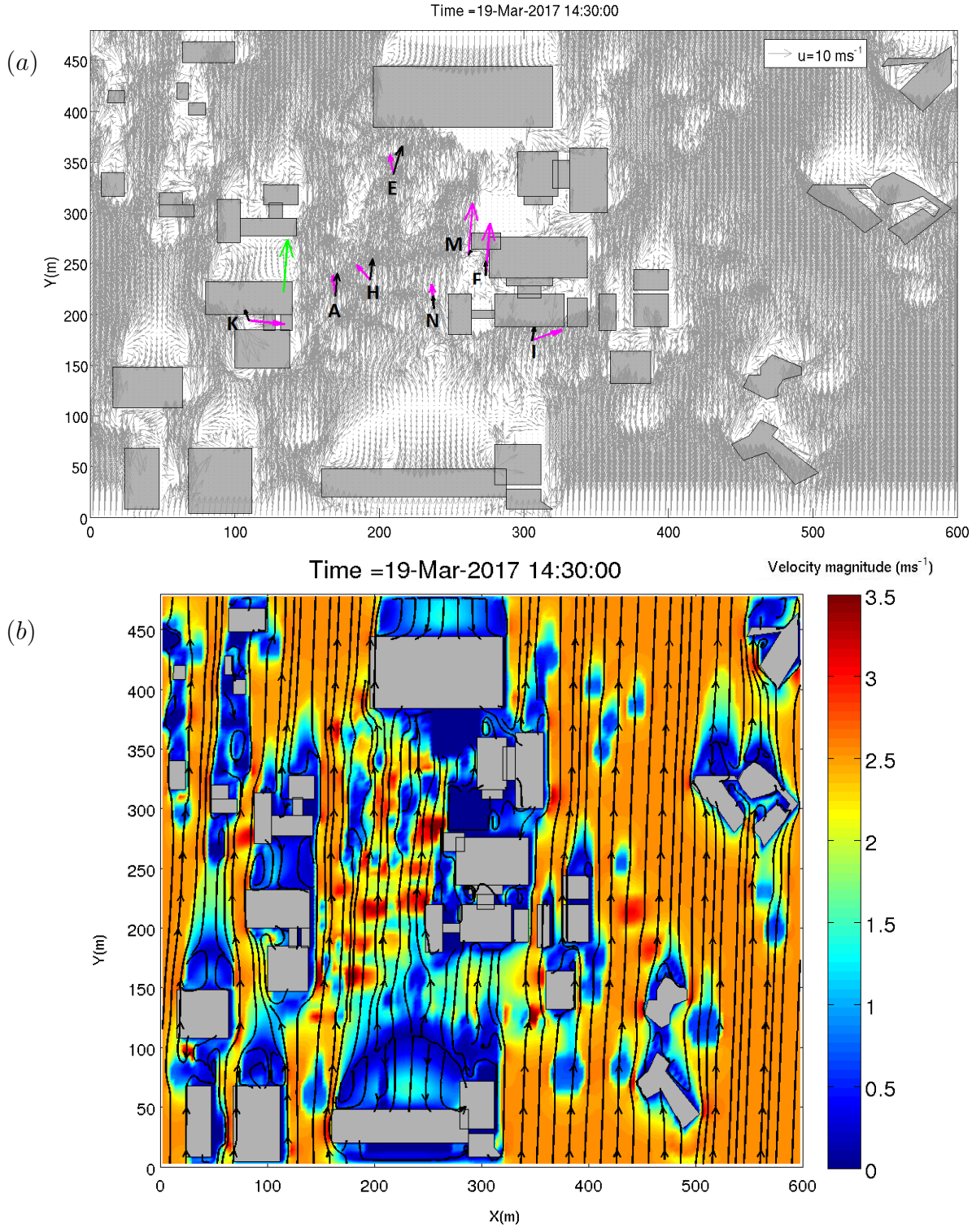

Figure 4.4. Qualitative comparison at 1.65 m above ground for Case A with southerly wind speed of 4 ms^{-1} at the reference height of 36 m above the ground at the WBB building. a) Velocity vector plot. The green, black, and magenta vectors are the reference vector, QUIC-URB results, and experiment winds measured with LEMS, respectively. b) Velocity magnitude contour and streamline plot.

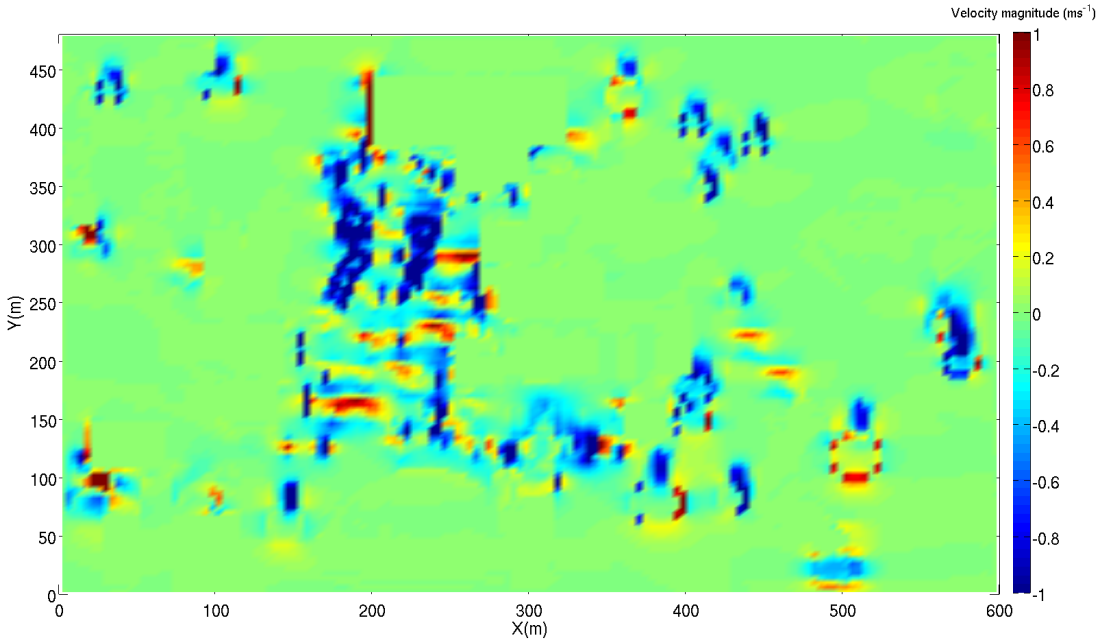

Figure 4.5. Contour plot of velocity magnitude difference between the vegetation wake and original QUIC-URB model(Cionco) for Case A: 19 March 2017 at 14:30 at 1.65 m above ground.

(a)

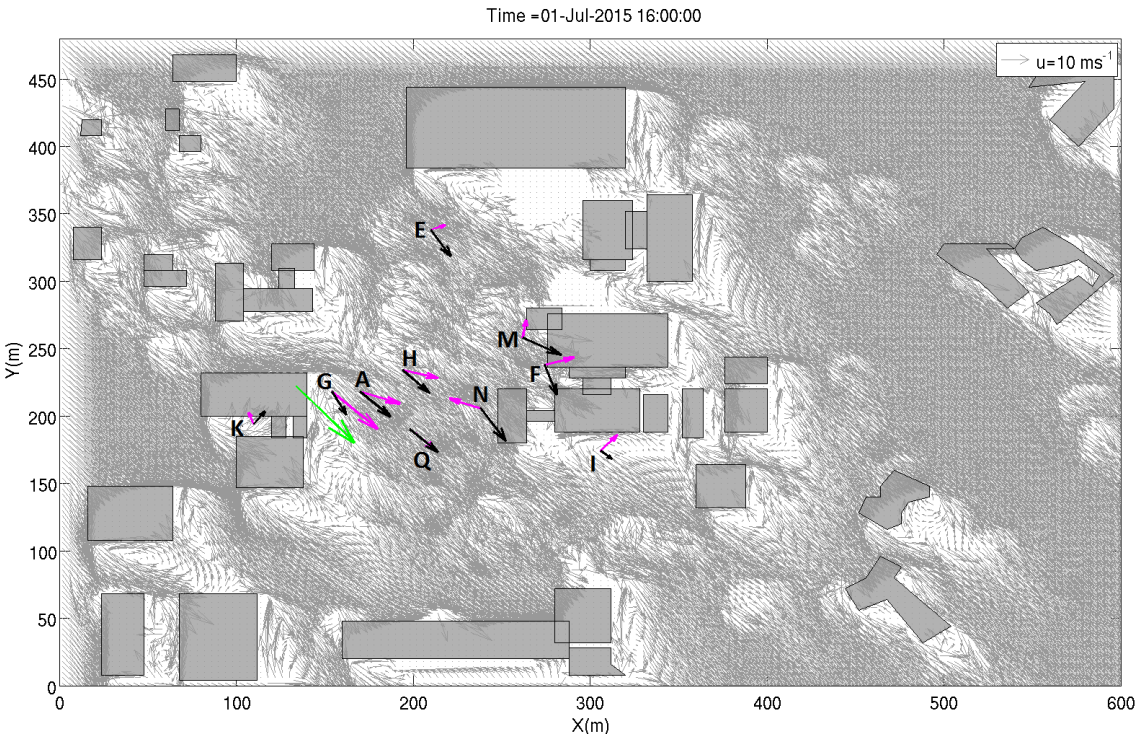

(b)

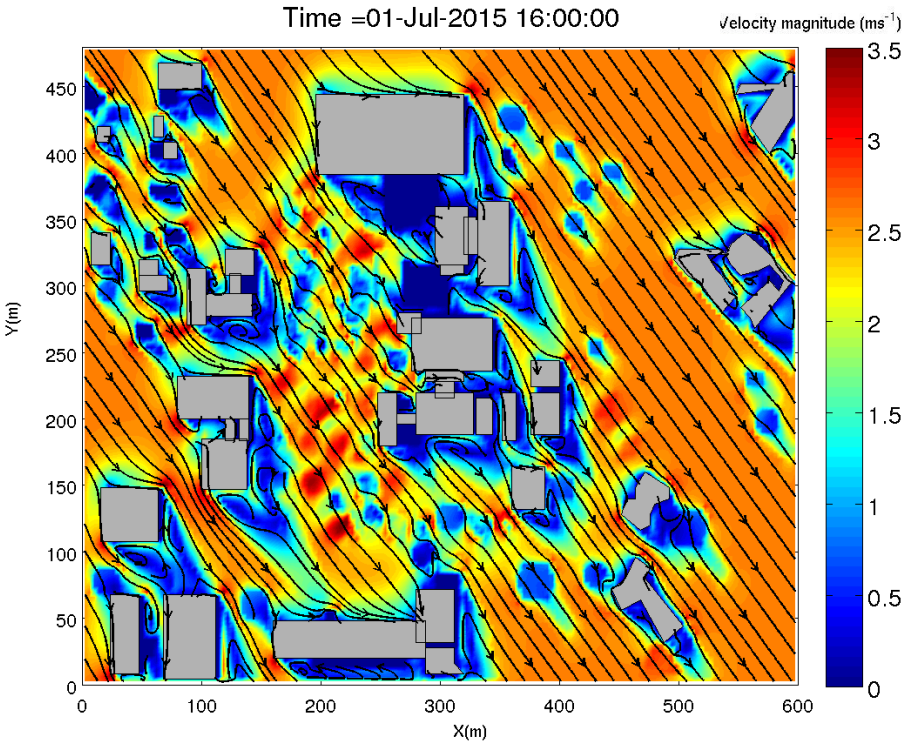

Figure 4.6. Qualitative comparison at 1.65 m above ground for Case B with wind speed of 5.6 ms^{-1} at the reference height of 36 m above the ground. a) Velocity vector plot. The green, black, and magenta vectors are the reference vector from the top of the WBB building, QUIC-URB results, and experiment winds, respectively. b) Velocity magnitude contour and streamline plot.

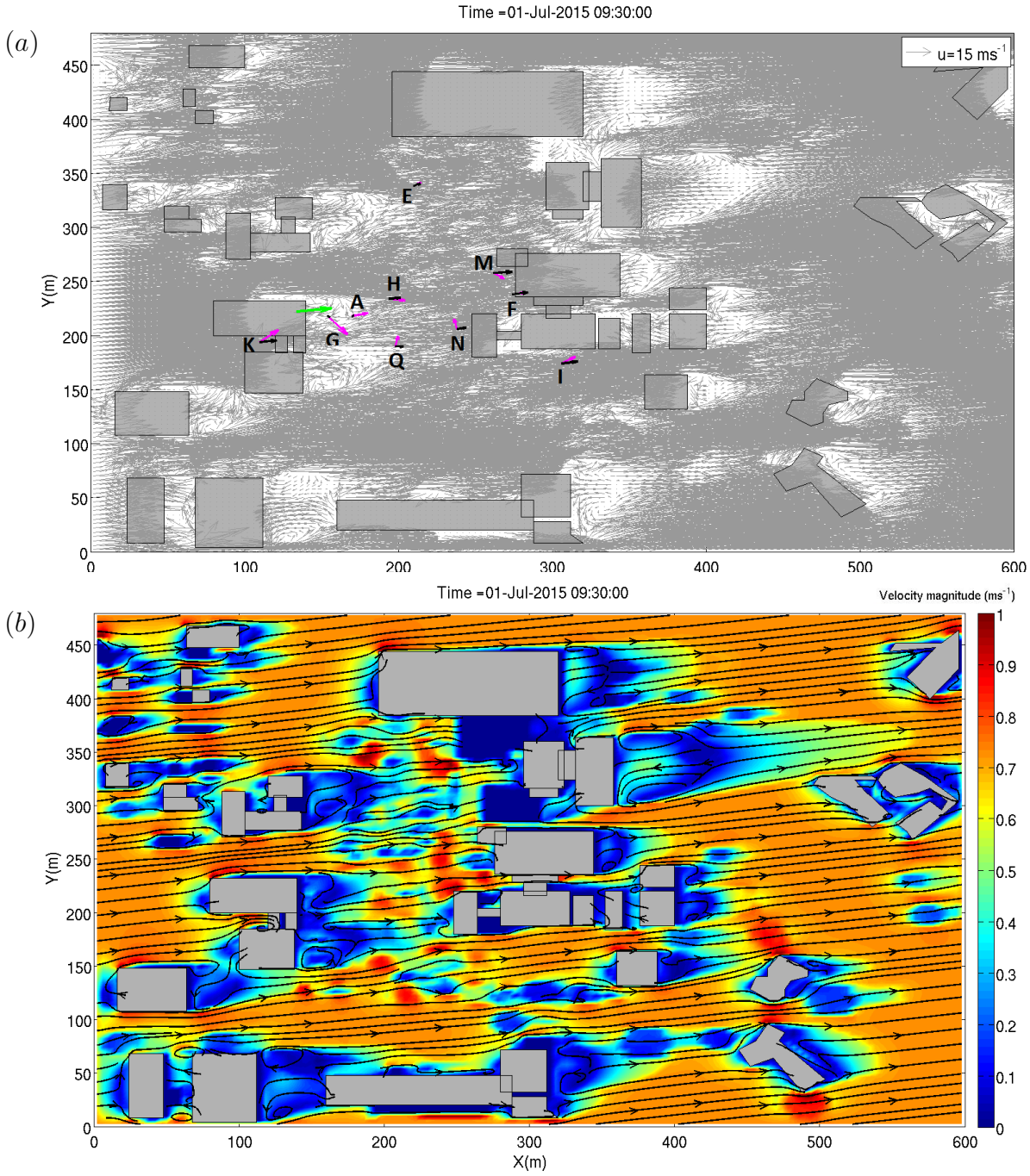

Figure 4.7. Qualitative comparison of QUIC-URB with the vegetation wake model and experimental data for Case B: 1 July 2015 at 9:30 with wind speed of 2 ms^{-1} at the reference height of 36 m above the ground. The buffer region is eliminated in figures. a) Velocity vector plot at 1.65 m above ground. The green vector is the reference vector from the top of the WBB building, black vectors are QUIC-URB results, and magenta vectors are experiment winds. b) Velocity magnitude contour and streamline plot at 1.65 m above the ground.

(a)

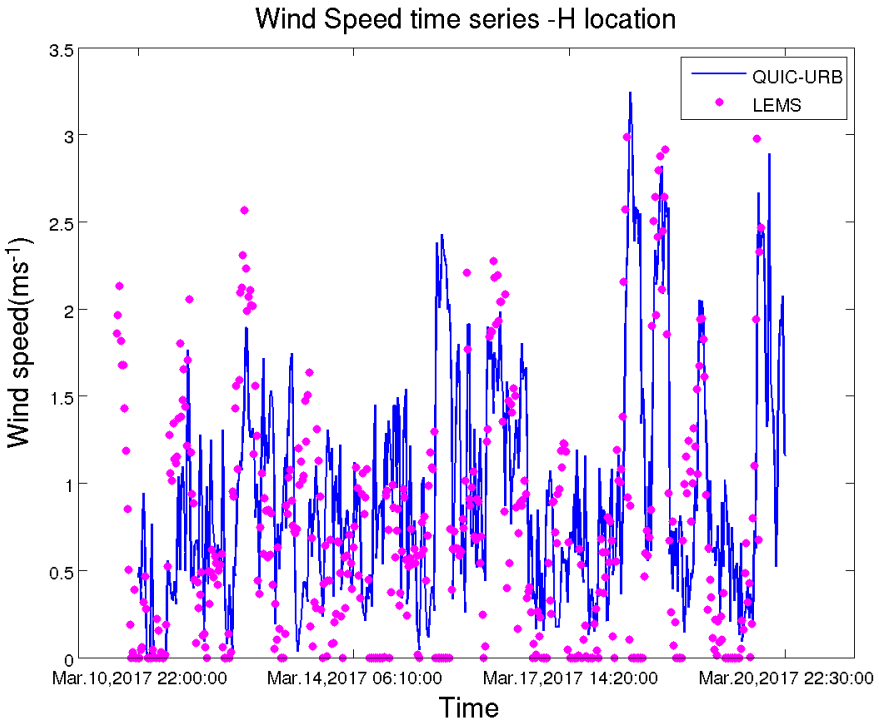

(b)

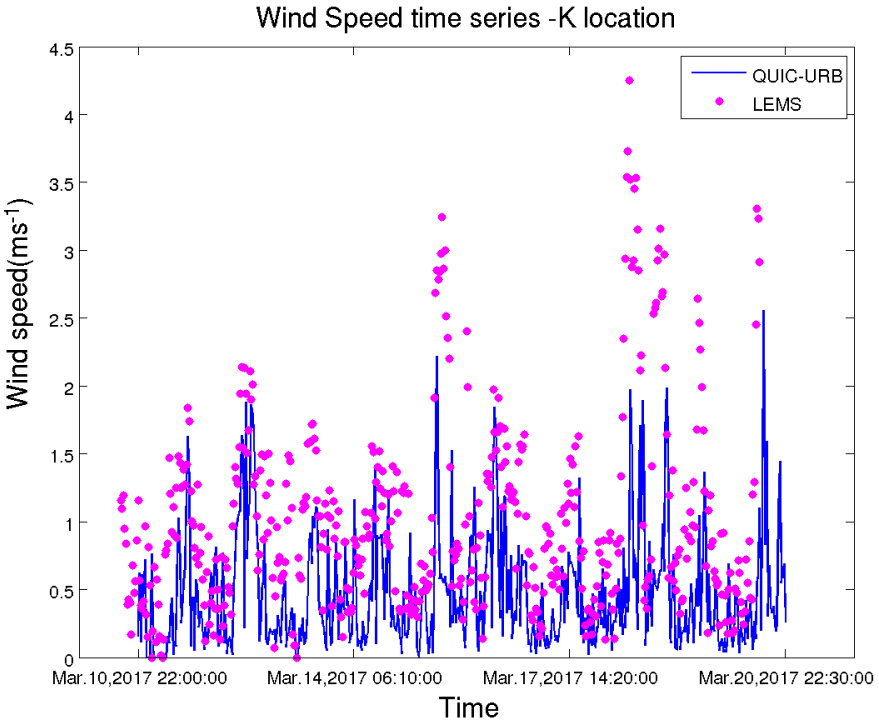

Figure 4.8. Qualitative comparison of QUIC-URB with the vegetation wake model and experimental data during Case A. a) Wind speed time series on LEMS H location for case A. b) Wind speed time series on LEMS K location for case A.

(a)

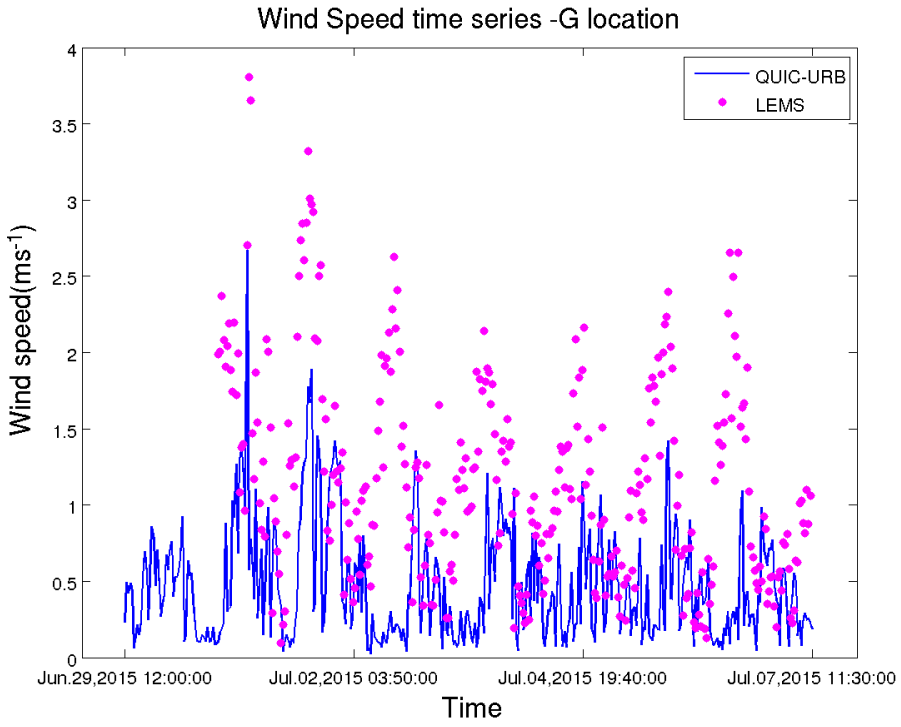

(b)

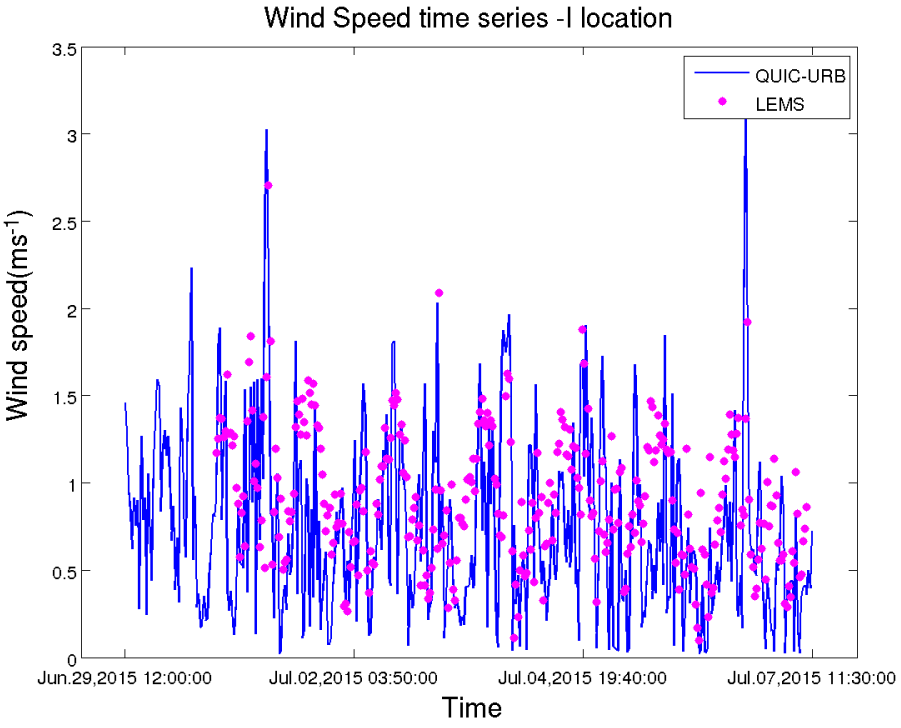

Figure 4.9. Qualitative comparison of QUIC-URB with the vegetation wake model and experimental data during Case B. a) Wind speed time series on LEMS G location for case B. b) Wind speed time series on LEMS I location for case B.

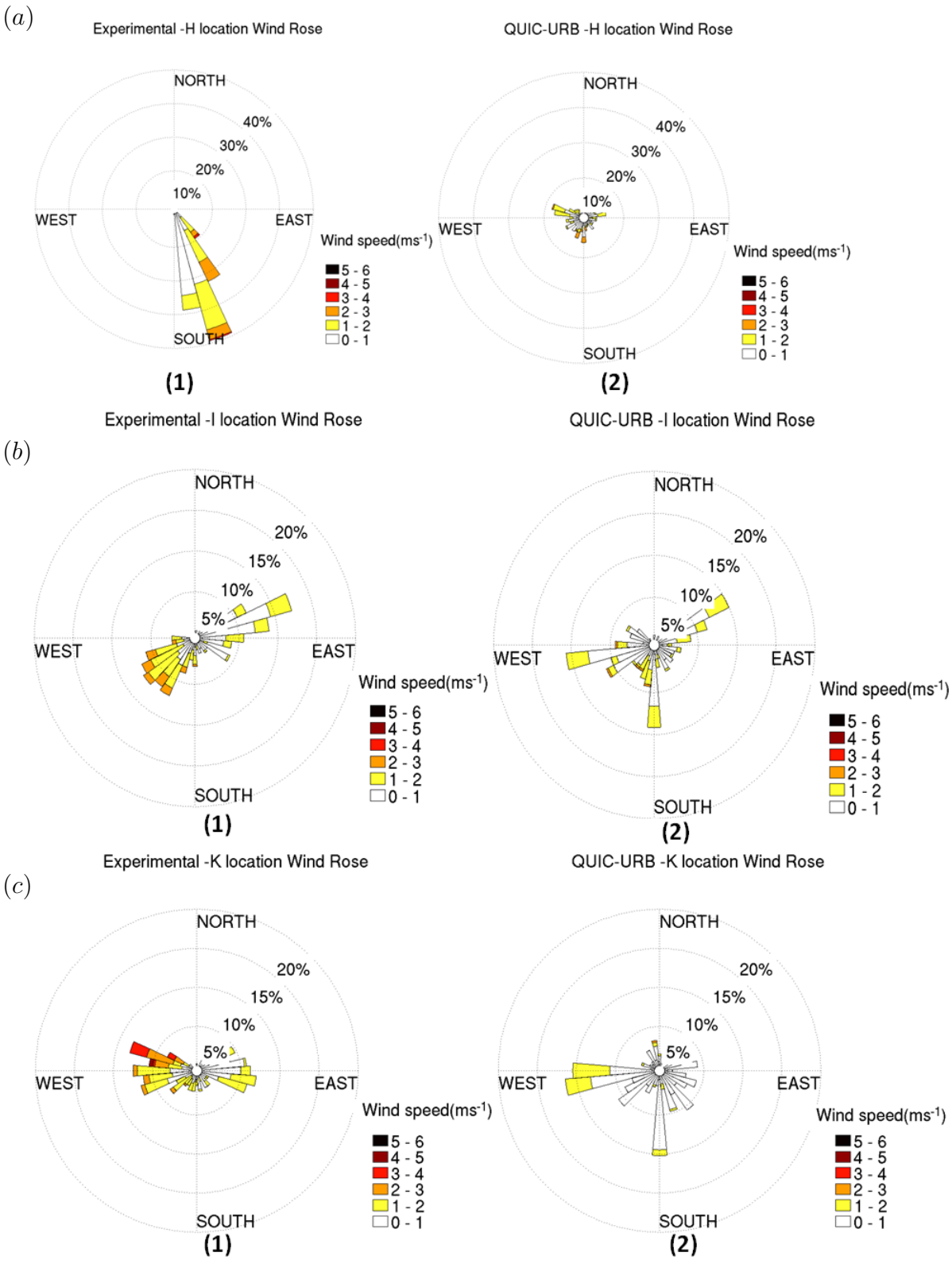

Figure 4.10. Quantitative comparison of experimental data (1) and QUIC-URB with the vegetation wake model (2) during case A (19-28 March 2017) with wind rose at: a) LEMS H, b) LEMS I, and c) LEMS K locations.

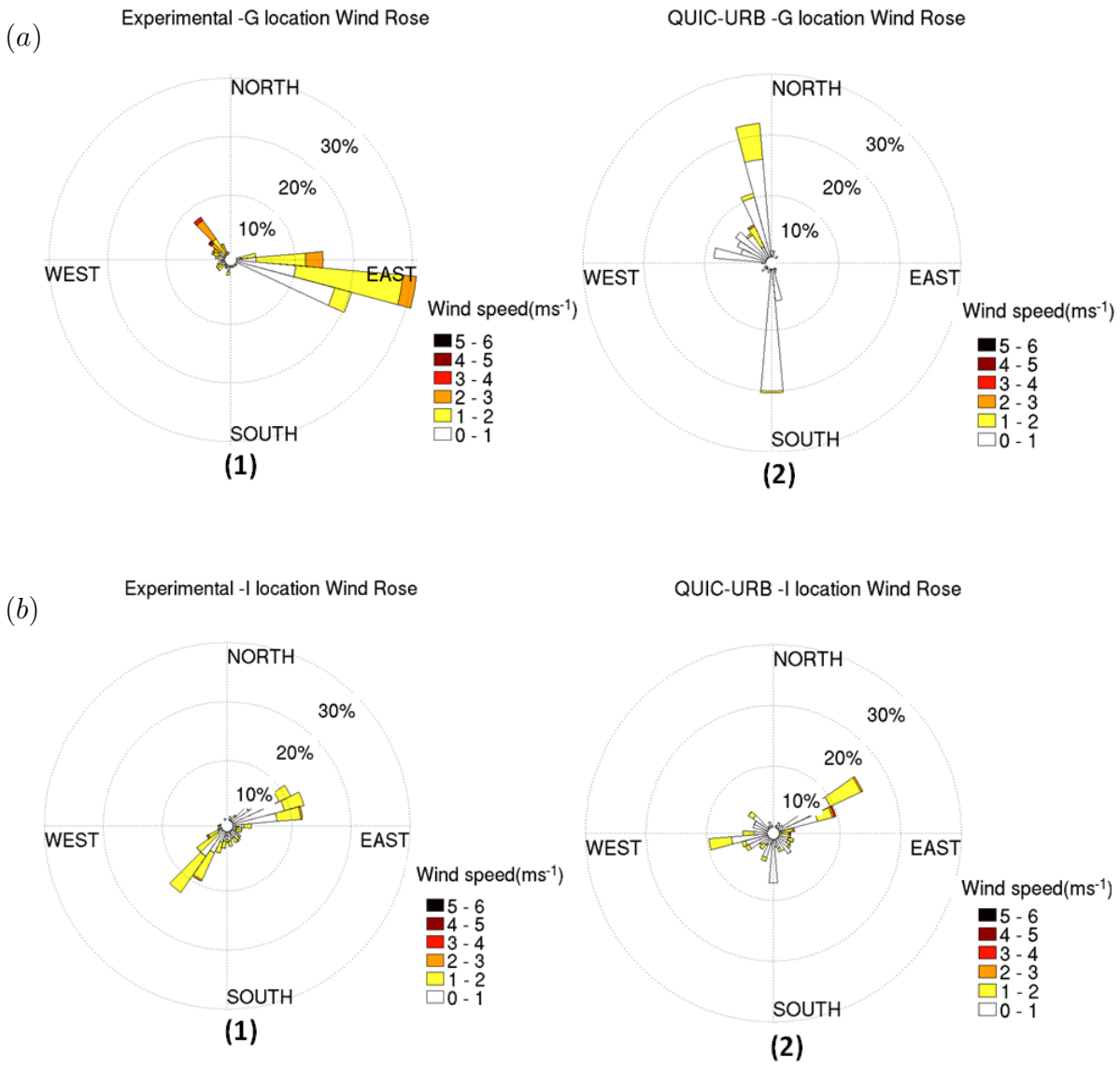

Figure 4.11. Quantitative comparison of experimental data (1) and QUIC-URB with the vegetation wake model (2) during Case B (29 June to 7 July 2015) with wind rose at: a) LEMS G b) LEMS I locations.

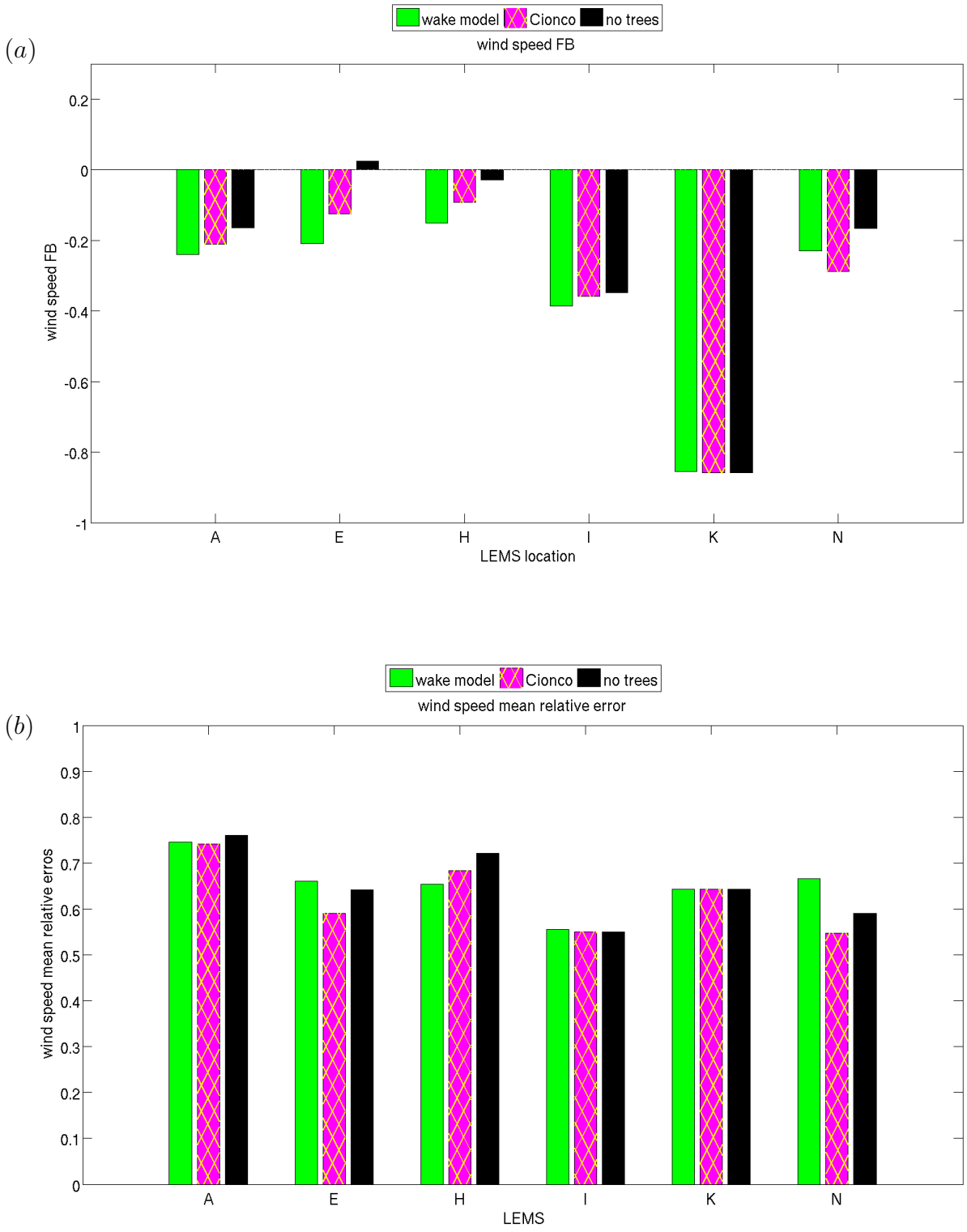

Figure 4.12. Quantitative comparison of QUIC-URB with the vegetation wake model and experimental data for case A (19-28 March 2017): a) Fractional bias comparison, b) Mean relative error comparison

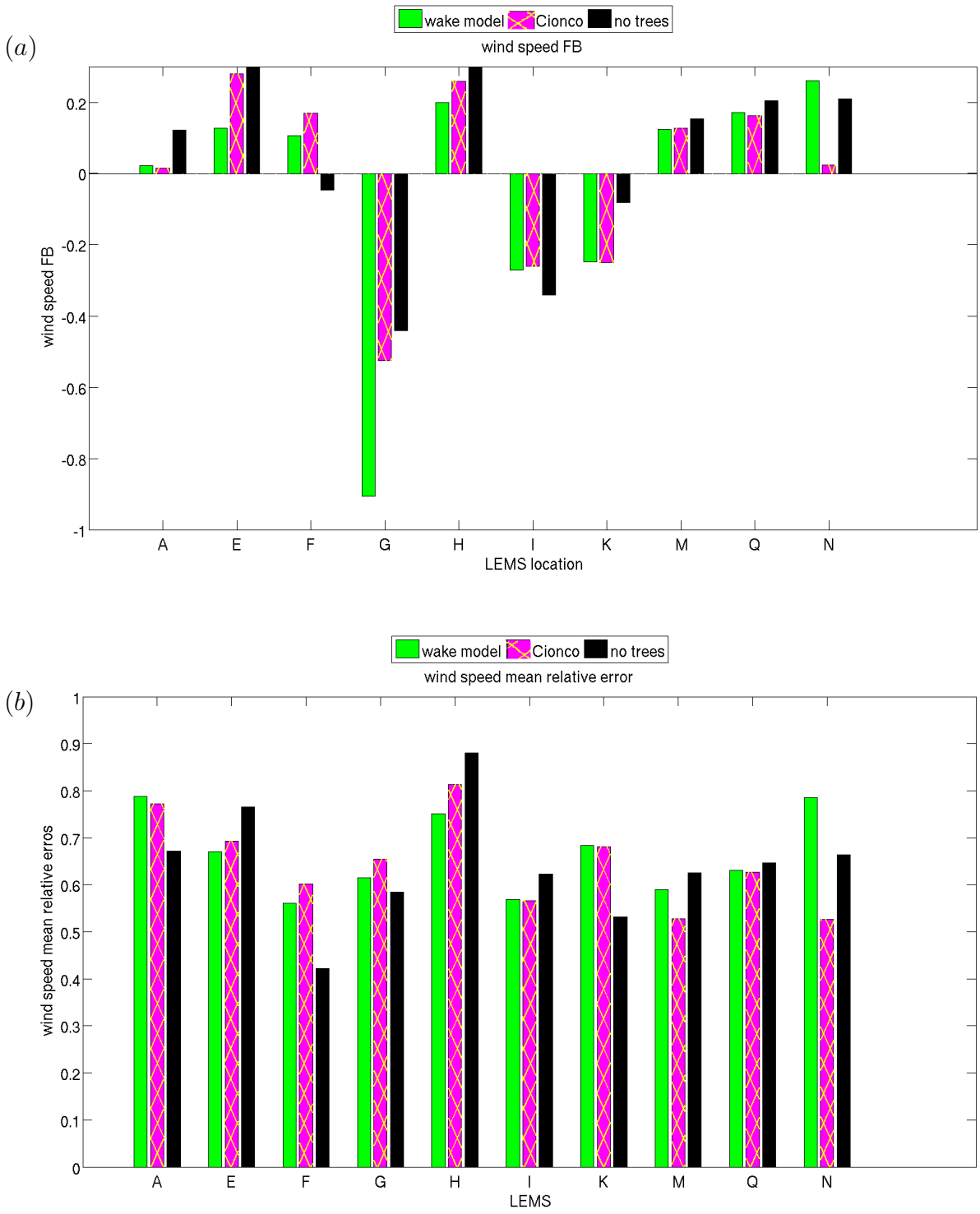

Figure 4.13. Quantitative comparison of QUIC-URB with the vegetation wake model and experimental data for case B (29 June to 7 July 2015): a) Fractional bias comparison, b) Mean relative error comparison

(a)

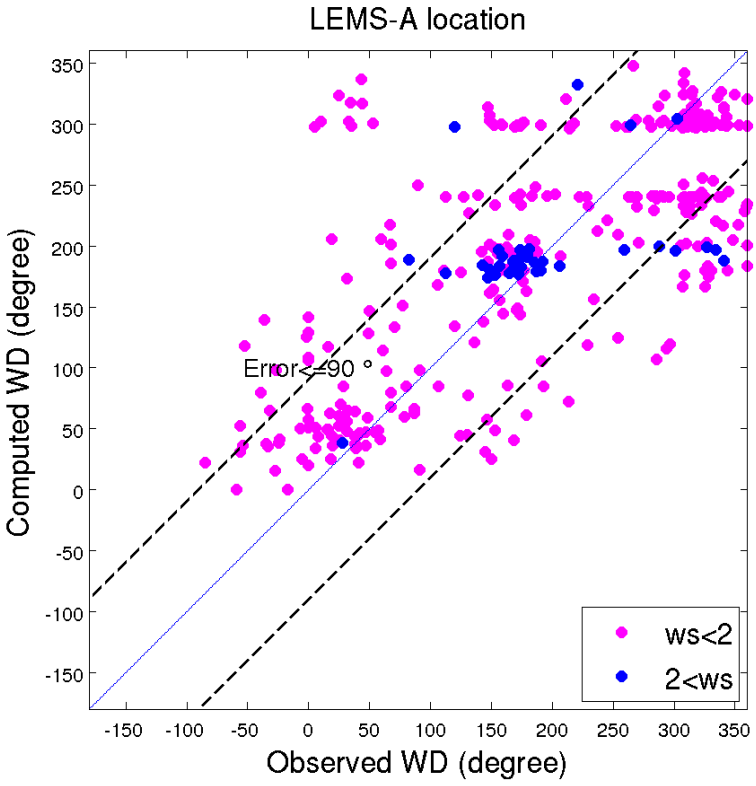

(b)

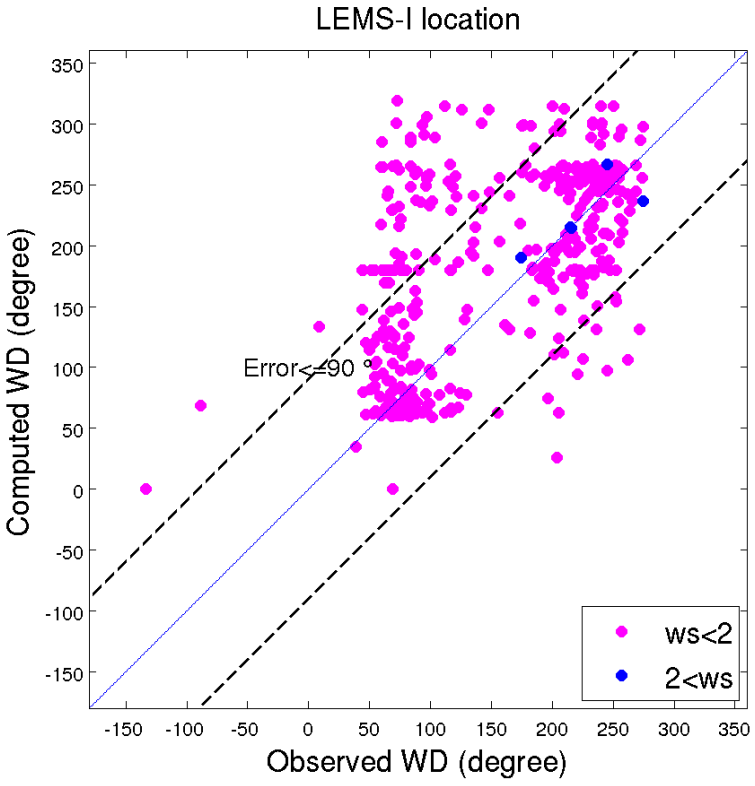

Figure 4.14. Quantitative comparison of QUIC-URB with the vegetation wake and experimental data for case A (19-28 March 2017) a) LEMS A (r^2 = 0.46) and b) LEMS I (r^2 = 0.31).

(a)

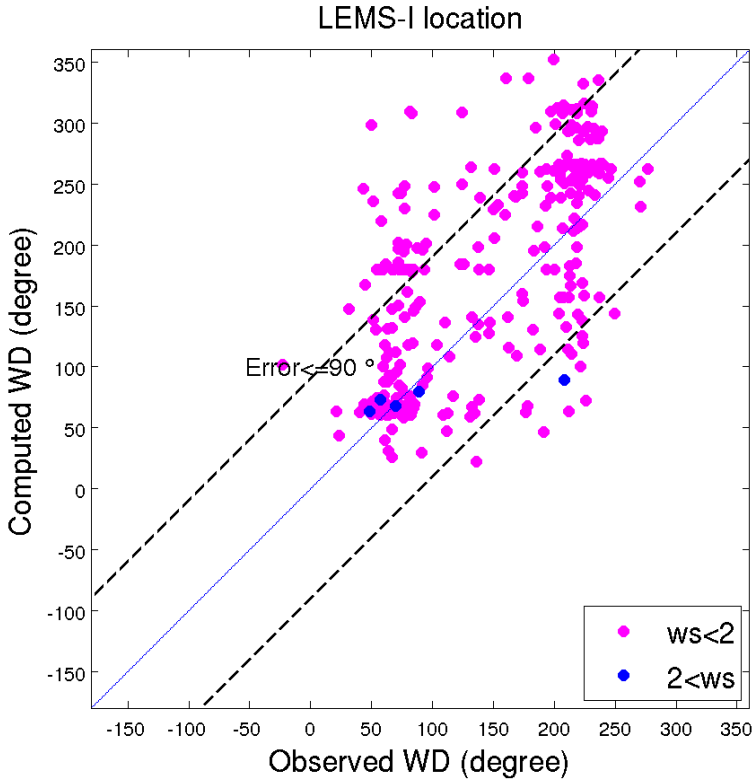

(b)

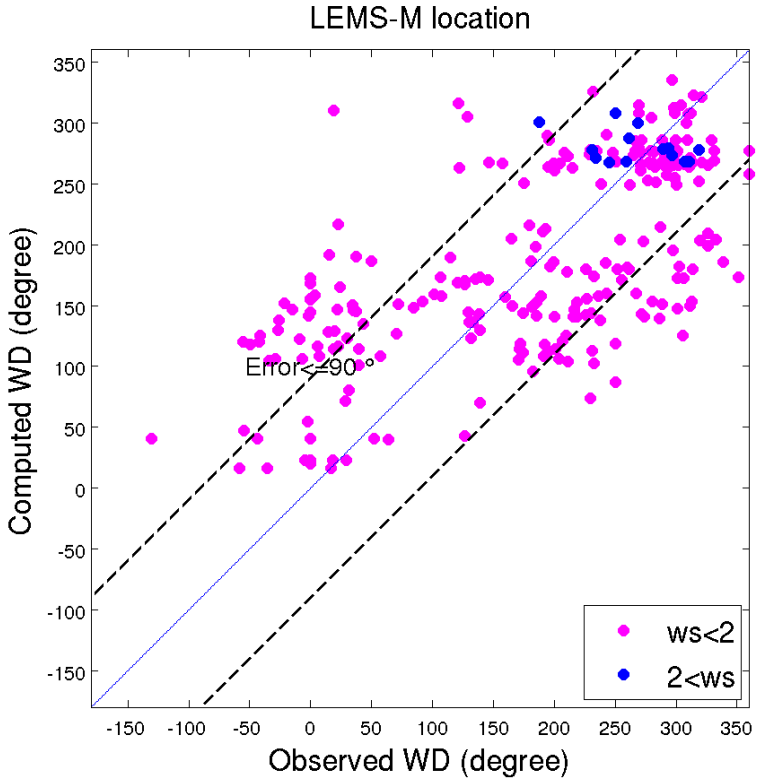

Figure 4.15. Quantitative comparison of QUIC-URB and experimental data for case B (29 June to 7 July 2015). a) LEMS I ($r^2 = 0.45$) and b) LEMS M ($r^2 = 0.44$).

4.5 References

C.S.B. Grimmond, T. O., 1998: Aerodynamic properties of urban areas derived from analysis of surface form. *Journal of Applied Meteorology*, **38**, 1262–1292.

Girard, P., D. F. Nadeau, E. Pardyjak, M. Overby, P. Willemsen, R. Stoll, B. Bailey, and M. Parlange, 2017: Validation of the QUIC-URB wind solver and qesradiation radiation-transfer model using a dense array of urban meteorological observations. *Urban Climate*, **submitted**.

Google Earth, 2016: University of Utah 40.7649 n, 111.8421 w. URL https://www.google.com/earth/index.html, online; accessed May 1, 2017.

Gowardhan, A. A., E. R. Pardyjak, I. Senocak, and M. J. Brown, 2011: A CFD-based wind solver for an urban fast response transport and dispersion model. *Environmental Fluid Mechanics*, **11 (5)**, 439–464.

Gunawardena, N., E. Pardyjak, R. Stoll, and A. Khadka, 2017: Development and evaluating an open-source low-cost distributed sensor network for environmental monitoring applications. *Measurement Science and Technology*, **in-preparation**.

MesoWest, 2017: University of Utah. URL http://mesowest.utah.edu/, online; accessed May 1,2017.

Neophytou, M., A. Gowardhan, and M. Brown, 2011: An inter-comparison of three urban wind models using Oklahoma City joint urban 2003 wind field measurements. *Journal of Wind Engineering and Industrial Aerodynamics*, **99 (4)**, 357 – 368, the Fifth International Symposium on Computational Wind Engineering.

CHAPTER 5

CONCLUSION

In this paper, we have investigated and evaluated various modeling strategies that can be used to better understand the effects of vegetation in urban environments. The main focus of this work was the development of a vegetation wake model that accounts for flow physics in the bleed zone and wake of an idealized isolated tree. A new mathematical model for an isolated tree wake was implemented into the empirical mass-conserved QUIC-URB model to compute the velocity deficit in wake and bleed zones. The model has been validated against published wind-tunnel studies of flow through and around a single tree. Although the validation shows disagreement in very close proximity ($x/h < 2$) to the tree for high LAIs (> 3.3), farther downstream of vegetation, wake model results show good agreement where relative errors were less than 15% and valuable potential for wind field modeling purposes.

To evaluate the overall performance of QUIC-URB in a real complex urban environment, a field experiment was conducted at the University of Utah. Three simulations in QUIC-URB framework were performed: no trees, the Cionco model, and our newly implemented vegetation wake model. The experimental results included near-surface (2 m) level wind field data. These results were compared with simulations for two distinct time periods using 30 min time averaging. We have obtained comprehensive and fairly accurate results indicating the spatio temporal averaged wind speed relative error of 65 % for a fast-response simple CFD model in all configurations (no-trees, Cionco model, and with-trees models) compared to experimental data. However, for upwind and building wake, our investigation reveals that the QUIC-URB model underestimates wind field (FB ≈ -0.4) in these regions. Surprisingly, no significant differences were observed between no-trees and with-trees

cases. The experimental setup was limited. Due to battery charging requirements, sensors needed to be sited out of tree shading, leading to a bias in the placement of sensors away from vegetation. This study has contributed to enhance our understanding of QUIC-URB performance in cities with vegetation. Future work needs to be carried out to establish how different leaf area indices impact model performance. Further wind-tunnel and field studies are needed to establish this impact. More broadly, research is needed to examine field experiment data covering a larger time period and more conditions. Furthermore, for more detailed geometrical information of the simulated domain, more accurate land surveying methods such as Lidar should be undertaken. It is important to mention that the wake model is created based on the main assumption that the tree is isolated. When we apply the wake model, trees violating this assumption should be omitted from the simulations or a different approach should be considered. Additionally, the current version of QUIC-URB does not include the non-flat terrain. To consider this effect, parts of the domain with hills and steep terrain were modeled by stacks of small buildings to imitate the non-flat terrain. In addition, the experimental measurements were relatively far from these hills and may not have the impact of non-flat terrain. Therefore, the evaluation presented here could be used as a baseline for improving future vegetation parameterisations in QUIC-URB model.

APPENDIX

STATISTICAL METRICS

The metrics used for comparing QUC-URB vegetation wake model with field experiment were calculated using Eqs. A.1 to A.6 and shown in Figs. A.1 to A.4.

$$\text{Absolute Difference} = \frac{\sum_i^n |E(i) - S(i)|}{n} \tag{A.1}$$

$$\text{FB} = \frac{\overline{E} - \overline{S}}{0.5(\overline{E} + \overline{S})} \tag{A.2}$$

$$\text{Mean Error} = \sum_i^n \frac{|E(i) - S(i)|}{n} \tag{A.3}$$

$$\text{Mean Relative Error} = \sum_i^n \frac{|E(i) - S(i)|}{nS(i)} \tag{A.4}$$

$$\text{Normalized Absolute Difference} = \frac{\sum_i^n |E(i) - S(i)|}{\sum_i^n [E(i) + S(i)]} \tag{A.5}$$

$$\text{Normalized Mean Square Error} = \frac{\sum_i^n (|E(i) - S(i)|)^2}{\sum_i^n ([E(i) + S(i)])^2} \tag{A.6}$$

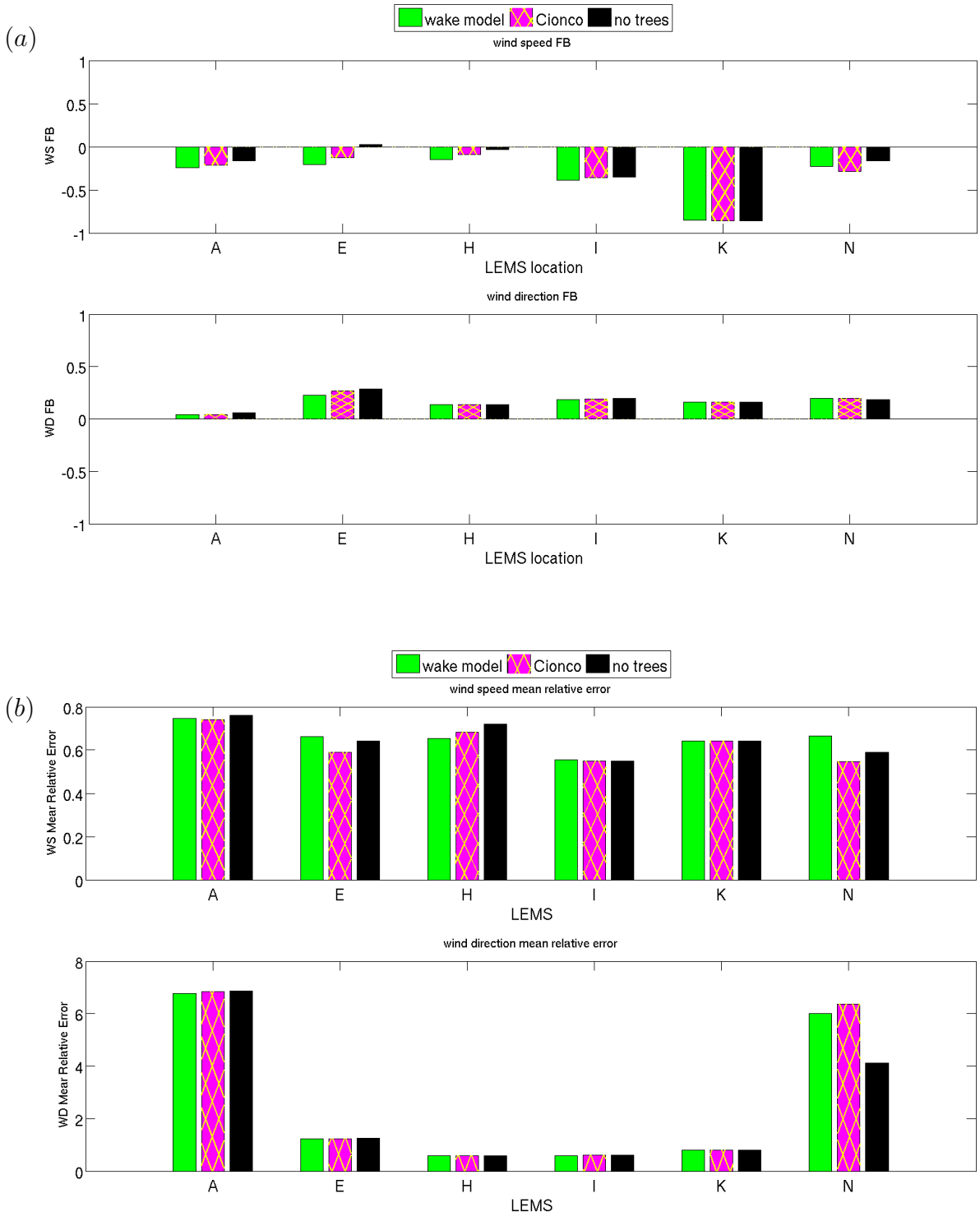

Figure A.1. Quantitative comparison of QUIC-URB with the vegetation wake model and experimental data for case A (19-28 March 2017): a) Fractional bias comparison, b) Mean relative error comparison

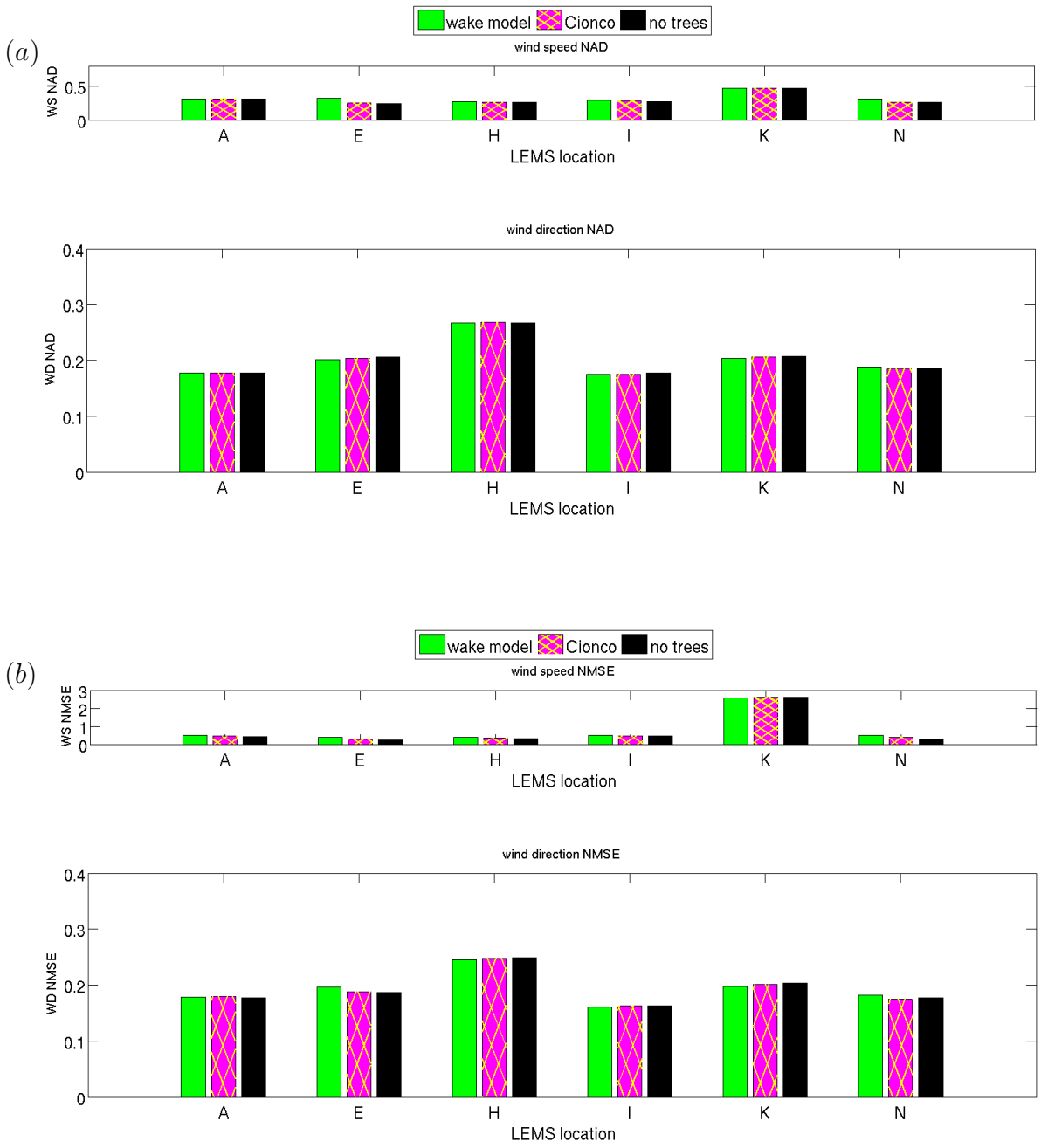

Figure A.2. Quantitative comparison of QUIC-URB with the vegetation wake model and experimental data for case A (19-28 March 2017): a) Normalized Absolute Error comparison, b) Normalized Mean Square Error comparison

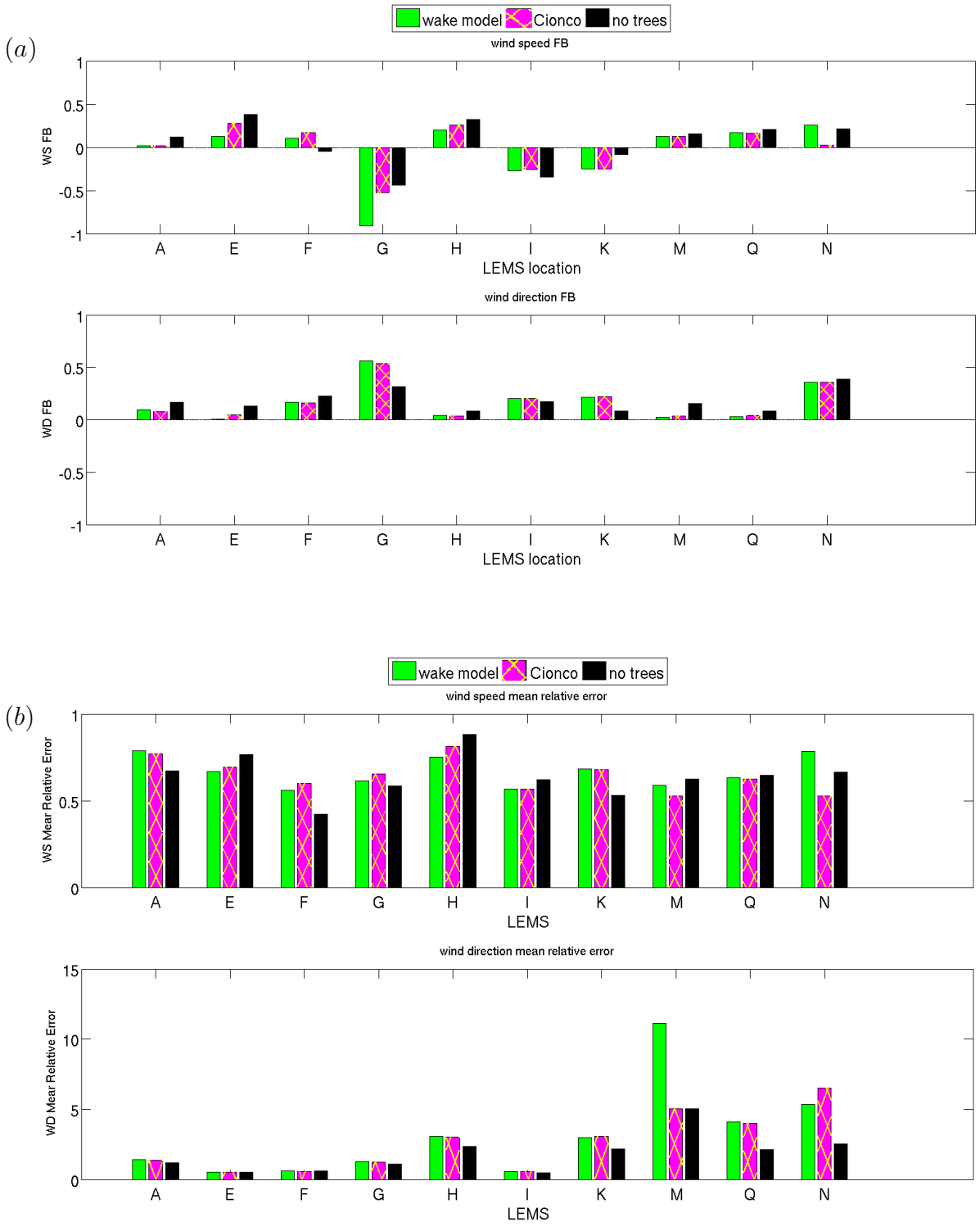

Figure A.3. Quantitative comparison of QUIC-URB with the vegetation wake model and experimental data for case B (29 June to 7 July 2015): a) Fractional bias comparison, b) Mean relative error comparison

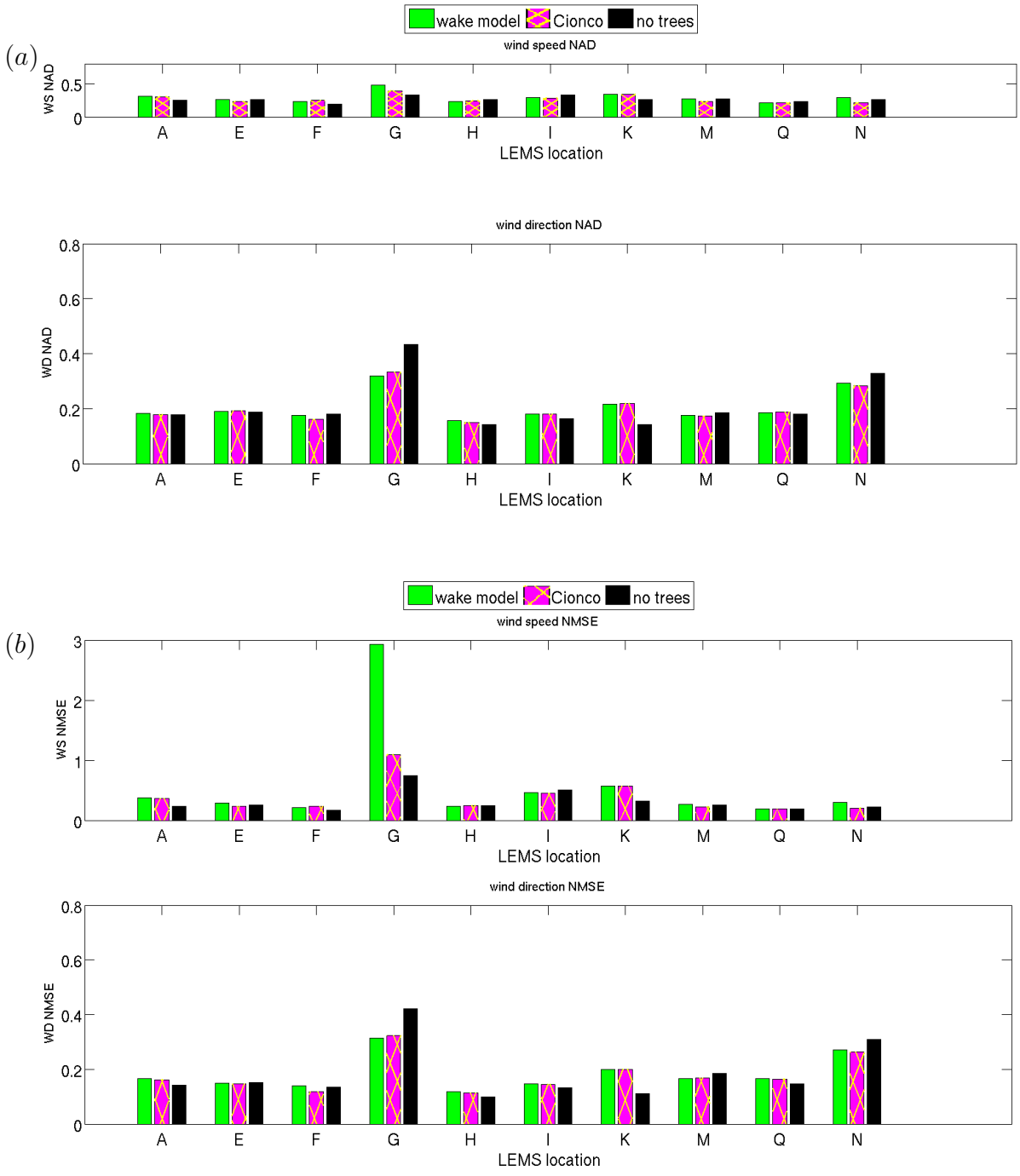

Figure A.4. Quantitative comparison of QUIC-URB with the vegetation wake model and experimental data for case B (29 June to 7 July 2015): a) Normalized Absolute Error comparison, b) Normalized Mean Square Error comparison